

Article

Not peer-reviewed version

Performance Evaluation of Small Wind Turbines under Variable Winds of Cities; Case Study Applied to an Ayanz Wind Turbine with Screw Blades

[Gonzalo Abad](#)^{*}, [Ander Plaza](#)^{*}, [Gorka Kerejeta](#)^{*}

Posted Date: 11 September 2024

doi: 10.20944/preprints202409.0842.v1

Keywords: Small-wind turbines; variable wind speed; wind at city locations; Maximum Power Point Tracking



Preprints.org is a free multidiscipline platform providing preprint service that is dedicated to making early versions of research outputs permanently available and citable. Preprints posted at Preprints.org appear in Web of Science, Crossref, Google Scholar, Scilit, Europe PMC.

Copyright: This is an open access article distributed under the Creative Commons Attribution License which permits unrestricted use, distribution, and reproduction in any medium, provided the original work is properly cited.

Disclaimer/Publisher's Note: The statements, opinions, and data contained in all publications are solely those of the individual author(s) and contributor(s) and not of MDPI and/or the editor(s). MDPI and/or the editor(s) disclaim responsibility for any injury to people or property resulting from any ideas, methods, instructions, or products referred to in the content.

Article

Performance Evaluation of Small Wind Turbines under Variable Winds of Cities; Case Study Applied to an Ayanz Wind Turbine with Screw Blades

Gonzalo Abad ¹, Ander Plaza ¹ and Gorka Kerejeta ¹

¹ Computer and Electronics Department, Mondragon University, 20500 Mondragon, Spain

* Correspondence: gabad@mondragon.edu

Highlights:

What are the main findings?

- It is found how small-wind turbines behave in terms of energy production, under the variable winds of city locations.
- It is found how does affect the power conversion system and control of small-wind turbines, to the maximization of energy production of small wind turbines.

What are the implications of the main finding?

- Thanks to these findings or analysis, it is possible to know for a given small wind turbine morphology, if a low-cost and simple power conversion configuration can produce more energy than a typical and more complex and expensive MPPT based power conversion configuration.
- Therefore, knowing this, it is possible to design more cost-effective wind turbines than traditional ones.

Abstract: Small wind turbines placed at City locations are affected by variable speed winds that frequently also change the direction. Architectural constructions, buildings of different height and abrupt orography of Cities make the winds that occur at City locations, more variable than in flat lands or at sea. However, performance of Small-wind turbines under this type of variable winds is not deeply studied in specialized literature. Therefore, this article analyses this important issue, also considering three types of power conversion configurations utilized in small-wind turbines; the generally used Maximum Power Point Tracking (MPPT) configuration, the simple only-rectifier configuration and an intermediate configuration in terms of complexity called Pseudo-MPPT. This general-purpose analysis is applied to a specific type of wind turbine, i.e. the Ayanz wind turbine with screw blades, which presents very adequate characteristics for city locations such as; safety, reduced visual and acoustic impacts and birds' casualties avoidance. Thus, a wide simulation and experimental tests-based analysis is carried out, identifying which are the main factors affecting to the maximization of energy production of small-wind turbines in general and the Ayanz turbine in particular. It is concluded that depending how the wind turbine is designed in terms of these identified main factors, the simple Pseudo-MPPT power conversion configuration could even extract more energy than more complex MPPT configurations, especially in quickly varying wind situations.

Keywords: small-wind turbines; variable wind speed; wind at city locations; power conversion configuration; maximum power point tracking (MPPT); Ayanz wind turbine with screw blades; equivalent inertia

1. Introduction

In this day and age, global warming and climate change have become critical problems which demand innovative and sustainable solutions in the energy field. This situation has prompted a transition towards renewable energy sources with the objective of reducing greenhouse gas emissions and promoting cleaner and safer electricity generation [1,2]. Generally, this transition has been dominated by large solar power installations, solar photovoltaic market has evolved from 70GW in 2011 to 942GW in 2021 [3]. Nevertheless, in recent years, interest has grown in self-consumption

technologies which will allow individuals and communities to generate their own electricity. This fact makes a decrease in their dependence on the conventional electrical network [4].

Solar photovoltaic energy has been the predominant technology in this area, due to the maturity of the market, the decreasing cost of solar panels, and the easy of installation in urban and residential environments [5]. However, small-scale wind energy (small wind turbines, SWT) is becoming a complementary option [6]. This type of energy has lots of advantages, especially in regions where wind resource is abundant and solar conditions are not as good as others. Also, while the PV panels work well in summer, their efficiency downgrades the rest of the year. For the wind turbines the situation is different, as the sun doesn't affect them, they give a more regular energy quantity during all the year [7]. Despite the growing interest in these technologies, research in SWTs is not so evolved and there are few studies which extensively analyse their performance in real urban wind conditions.

In general, smart cities require a lot of studies to be conducted. For instance, in [8] a study is made around the energy management in residential microgrids, in [9] a study in data-driven reliability prediction for district heating networks is made, and in [10] research is made on characterizing smart cities based on artificial intelligence. As a result of all these studies and evolution on smart cities, the development of urban wind turbines presents multiple technical and economic challenges. First, it is essential that these turbines are cost-effective compared to the PV technologies, which have seen an appreciable cost reduction over the last decade. This cost has fallen to a point that to produce 1W only 0.5\$ are needed [11]. Moreover, it is very important that SWTs offer stable and efficient performance in urban wind conditions, which are often turbulent and with fluctuating speeds [12]. Although the interest in these technologies is growing, there is no further research done in SWTs and there are few studies done in relation with their performance in real urban conditions [13].

A very important part of wind turbine is the power generation conversion system. Depending on this power electronic circuit, a given wind turbine morphology is able to extract more or less power from the wind. There are 3 main power configurations which are going to be analysed during this article: only rectifier topology, Pseudo-MPPT topology and MPPT topology [14]. The reason for analysing these is that there is no research done about which of the three is the best. Furthermore, no research has been done testing all of them against urban wind environment and more specifically, against different urban wind environment at changing conditions [15]. Also, there is little research done about which of the two main turbine topologies is the best for city environments (VAWT or HAWT) [16,17]. The objective is also to give data and information about this topic.

Then, focusing on this mentioned topic and with the idea for the commercial development of the small wind turbine research topic, one of the patents granted in 1606 to the distinguished inventor Jerónimo de Ayanz y Beaumont from Spain has been taken as a design reference [18,19]. This patent claims the use of a wind turbine based on screw blades, with a structure around it to channel or enclosure the wind. Having this known and using a commercial wind turbine based on Archimedes screw blades (Liam F1 AMW-750-D-150W, SC Respect, The Nederland, [20]), a built Ayanz wind turbine has been used for all the tests. This blade morphology has been widely studied for instance in [21]-[25]. Besides, this topology has been used due to its positive aspects such as its C_p value, the noise reduction (due to relatively low rotation speeds), start up and operation at low wind speeds, the ease of construction, the visual impact (due to the tube) and the avoidance of bird deaths due to the frontal net mounted on it [26]. This mentioned wind turbine can be seen in Figure 1. Knowing this, it has been decided to test this wind turbine in different wind gust scenarios based on real wind measurements taken in the urban area of Mondragon city (different speeds, orientations and repetitive gusts).

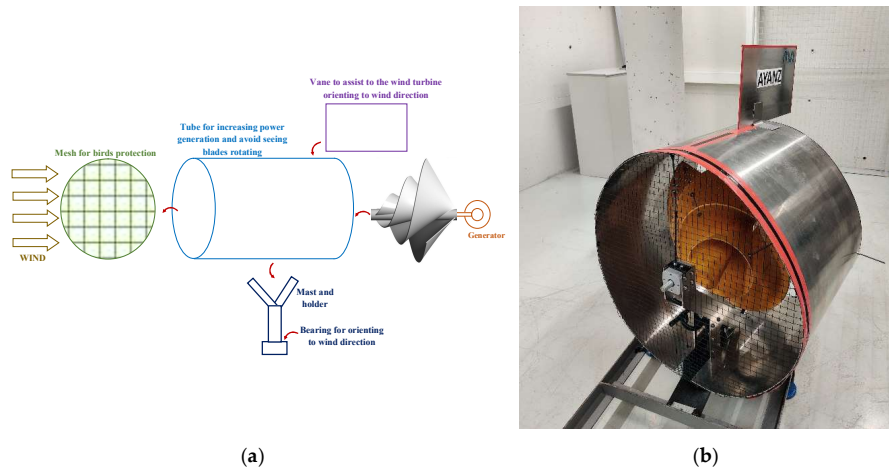


Figure 1. The Ayanz Wind Turbine based on Screw Blades. (a) Graphical scheme showing its main parts, (b) Prototype developed at Mondragon University, based on the commercially available Liam F1 AMW-750D-150W wind turbine and a cylindrical enclosure made of aluminium [20].

Finally, it is important to highlight that, although there are other studies which have explored the design and application of SWTs in urban environments, none has addressed as specifically as the present work, the performance analysis with real urban wind data [27]. This analysis aims to fill a significant gap in the current literature, providing a solid foundation for future research and development of small-scale wind technologies that are truly effective and sustainable in the field of urban self-consumption [28].

2. Horizontal Axis wind Turbine Used in This Study

2.1. The Ayanz Wind Turbine with Screw Blades

As commented earlier, the original patent of Ayanz inventor published in year 1606 [18,19], provides us a horizontal axis wind turbine with screw blades and then, blades are within an enclosure with cylindrical shape. This cylindrical enclosure, allows the capacity of the blades to capture more energy from the wind [26], together with some other practical advantages. Figure 1 graphically illustrates the wind turbine prototype developed at Mondragon University, using the commercially available Liam F1 AMW-750D-150W wind turbine. It uses the well-known Archimedes Spiral Wind Turbine [29] as screw-bladed wind turbine.

This is a horizontal axis wind turbine so it needs to be oriented to the wind direction. A very quick and effective orientation is achieved with this turbine, thanks to the assistance of the vane located at the bottom of the cylindrical enclosure, together with the fact that this turbine due to its morphology and geometry tends to self-orientate.

2.1. Main Characteristics of This Wind Turbine

The cylindrical enclosure of the wind turbine, enables to incorporate a metallic mesh at the input, avoiding birds entering to the inside of the wind turbine. This effective protection mesh prevents potential damages to the birds. In [26], it has been experimentally tested and demonstrated that if the mesh is sufficiently thin, it does not reduce the capacity of the turbine to capture energy from the wind, not affecting to its efficiency and aerodynamic coefficients. Then, thanks to the tube also, the visual impact and noise produced by the wind turbine is reduced. It should be noted that this enclosure considerably reduces the fact to continually see and hear the blades rotating, which is a fairly important benefit for many potential users who will install the wind turbines on the roofs of their homes. Finally, the tube also brings another advantage which is protection from potential damages at the blades. Note that if one blade is accidentally broken, safety of people or objects near the turbine is guaranteed, since the blade would not exit the tube. All these advantageous

characteristics are summarized at Table 1. On the other hand, the turbine presents the following geometrical characteristics [26]: 3 blades, effective radio of blades= 37.5 cm, radio of the tube =40.75cm, longitude=60cm, while the electric characteristics of the Permanent Magnet Synchronous Generator are: parasitic resistance = 9.56 Ω , parasitic inductance = 20.96 mH, ϕ_{pm} = 0.2665 Wb, pole pairs= 6.

Table 1. Main practical advantageous characteristics of the Ayanz Wind Turbine based on Screw Blades (at the end of the article, these characteristics are further explained and compared to other wind turbine morphologies).

| Main characteristic |
|---|
| It presents considerably high Cp coefficient so it is able to capture a significant portion of energy from the wind |
| reduction of the noise impact due to the tube and its moderately low rotational speed operation |
| minimization of the blades being watched rotating due to the tube |
| casualties in birds elimination due to the mesh |
| Safety provided by the tube since it protects from potential damages at the blades |
| Very fast Auto orientation due to its effective weathervane placed outside the blades |

To conclude, it has to be remarked that this wind turbine has been chosen for the study provided in this article, not only due to its above-mentioned benefits, but also because it is a horizontal axis wind turbine that needs to be oriented to the wind direction. As will be later shown, a study is carried out at the article, showing how the time the wind turbine needs to be oriented to the wind direction, impacts on the produced energy. Finally, it has to be remarked that for city locations, this is the one of the safest small wind turbines available (for surrounding objects, animals or persons) and also reduces considerably visual and acoustic impact, which are determinant facts to place small wind turbines at city locations where many people live nearby.

3. Power Conversion Configurations

3.1. Power Circuits and Controls

This section shows the three power conversion configurations for small wind turbines analysed in this paper [26]. These three power conversion systems are shown in Figure 2. The most general and complete conversion systems is presented above in the figure. It connects directly a diode-based rectifier to the AC generator, then a DC-DC conversion stage facilitates to implement a Maximum Power Point Tacking Algorithm (MPPT) and finally the electrical power generated is transmitted to a second stage that could be a battery, the electric AC grid or even a DC grid. For the MPPT consecution, it is necessary and specific control algorithm that is presented in next sub-section and consequently a micro-processor that enables its implementation.

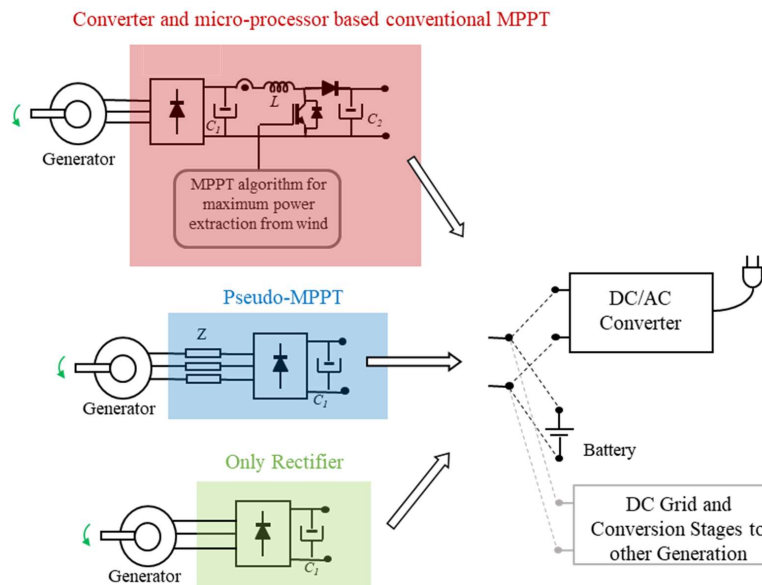


Figure 2. Most common power conversion configurations for small wind turbines [26].

Then, in Figure 2 below, another power conversion system is presented, which is based only of a diode-based rectifier and a DC capacitor for smoothing the output DC voltage. Compared with the previous configuration, this is a much simpler conversion concept since not DC-DC conversion system is used and therefore, not micro-processor is required. This type of conversion system is traditionally oriented to the smallest wind turbines and to low-cost wind turbine concepts.

Finally, a concept that is somewhere in the middle of the previous two ones in terms of complexity, is the one called as Pseudo-MPPT conversion system and it is shown at the middle in Figure 2. As can be noticed again, it incorporates a diode-based rectifier, the smoothing capacitor and an additional impedance that could be an inductance or a capacitance [26]. This concept, is tentatively conceived to be able to extract more power from the wind than the Only-Rectifier, but less than the Conventional or Ideal MPPT, with a power conversion system that does not require micro-processor, therefore reducing the complexity and losses of the power conversion system. This fact is schematically represented in Figure 3, where it is seen that at steady-state and constant wind speed conditions, theoretically, the Ideal MPPT is able to make the turbine operate at the peaks of the power curves at each wind speed (V_w). However, the Only-Rectifier concept since it operates at almost constant rotational speed (due to the nearly constant voltage operation of the generator imposed by the battery), is not able to work at the peaks of the power curves, generating less power. Finally, the Pseudo-MPPT concept, thanks to the voltage droop at the impedance located at output terminals of the generator, produces a slight variation at the voltage seen by the generator, producing also a slight variation of the mechanical speed, tentatively following better the power peaks of the power curves, as depicted in Figure 3. In subsequent analyses of the paper, for simplicity purposes, it will be supposed that the electric energy generated by the small wind turbine is evacuated to a battery. As can be noticed, left situation in Figure 3 shows a 'low voltage' battery chosen ('low' speed) for Pseudo-MPPT and Only Rectifier. On the contrary, Right situation shows a 'high voltage' battery chosen ('high' speed) for Pseudo-MPPT and Only Rectifier. At the left situation, the Pseudo-MPPT needs to increase the speed with higher winds, while at the right situation, the Pseudo-MPPT needs to decrease the speed with higher winds. Both situations are possible, depending on how all the elements of the system are chosen.

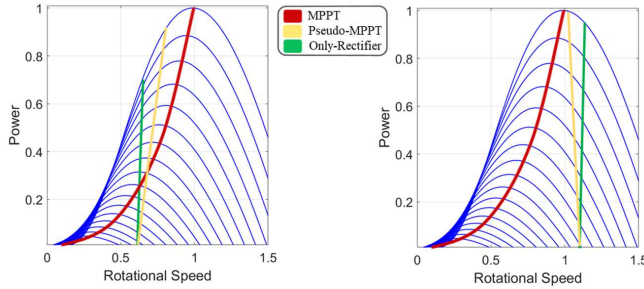


Figure 3. Tentative power generated, with the same wind turbine by the three power conversion configurations studied in this paper. Left situation shows a 'low voltage' battery chosen ('low' speed) for Pseudo-MPPT and Only Rectifier. Right situation shows a 'high voltage' battery chosen ('high' speed) for Pseudo-MPPT and Only Rectifier.

3.2. Indirect Speed Control based Conventional-MPPT

This section roughly explains how the Conventional-MPPT works in small wind turbines. There are several MPPT control algorithm versions [30], but in this article, a typically used one is used, i.e., the Indirect Speed Control based Conventional-MPPT [31,32]. The control block diagram is depicted in Figure 4.

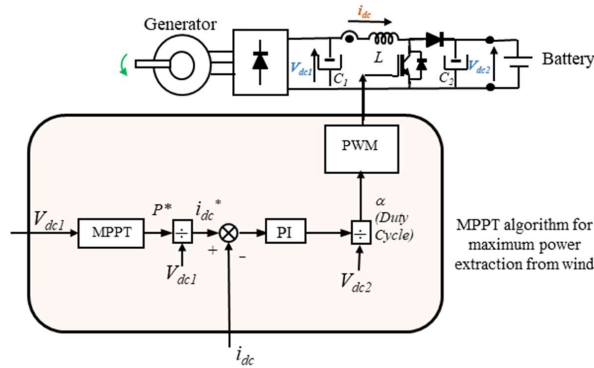


Figure 4. Indirect Speed Control based MPPT [31,32].

It is seen that the control generates the pulses for the controlled switch of the DC-DC converter. It depends on the how the elements of the specific system are designed, but in general, a Boost DC-DC converter is employed that increases the DC voltage from the input V_{dc1} to V_{dc2} , by means of the well-known equation:

$$\frac{V_{dc2}}{V_{dc1}} = \frac{1}{1-\alpha} \quad (1)$$

Being α the duty cycle for the controlled switch and V_{dc2} is imposed by the battery employed. This MPPT control, creates these pulses by only measuring two variables; V_{dc1} and i_{dc} . The fact of avoid needing to measure the rotational speed with a sensor, is advantageous for simplicity and reliability purposes of practical and successful wind turbines.

Then, the AC generator which normally is a Permanent Magnet Synchronous Generator, converts the mechanical energy extracted by the turbine from the wind, into electric energy. The single-phase equivalent circuit of the Synchronous Generator is depicted in Figure 5.

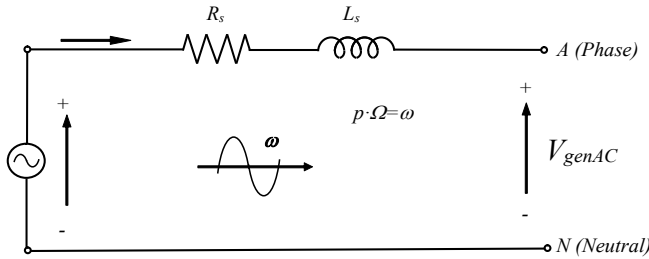


Figure 5. Synchronous generator's single phase equivalent circuit.

As noticed, neglecting the voltage droop at the parasitic resistance and inductance of the generator, at its terminals, sinusoidal three phase voltages appear with approximated amplitude (Phase-to-Neutral voltage):

$$|V_{gen}|_{LN} \cong \omega |\Psi_r| \quad (2)$$

These voltages are the input voltages of the diode-based rectifier, which converts the three phase AC voltages into DC output voltage as schematically represented in Figure 6.

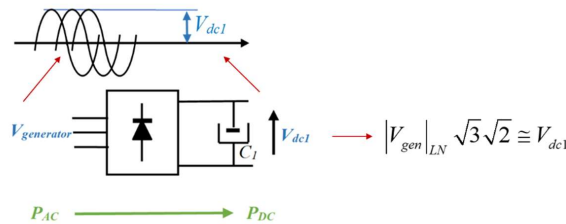


Figure 6. AC-DC conversion stage.

Thus, the DC voltage that appears at the input of the DC-DC converter is approximately as follows:

$$V_{dc1} \cong p\Omega |\Psi_r| \sqrt{3} \sqrt{2} \quad (3)$$

Which is indeed a voltage that is proportional to the rotational speed. Thus, taking advantage of this fact, the speed sensor is avoided.

Then, as commented before, the speed of the control performed by this MPPT version is an indirect speed control version. Thus, the rotational speed of the turbine is controlled indirectly without speed sensor. The generator is in charge of imposing an electromagnetic torque T_{em} , which follows the maximum power points curve ($T=k\Omega^2$ and $P=k\Omega^3$). While the torque created by the turbine T_t , follows the turbine torque curves at different wind speed as illustrated in Figure 7. Consequently, the turbine reaches naturally a steady-state equilibrium, at a rotational speed that follows the maximum points of the power curves.

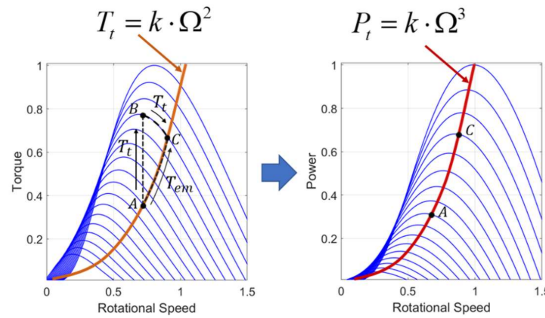


Figure 7. Indirect speed control of the wind turbine by imposing an electromagnetic torque T_{em} , which follows the maximum power points curve [31,32].

Hence, the electromagnetic torque T_{em} , is controlled by controlling the power as illustrated in Figure 8 (note that power and torque are related by the rotational speed and if one is controlled the other too).

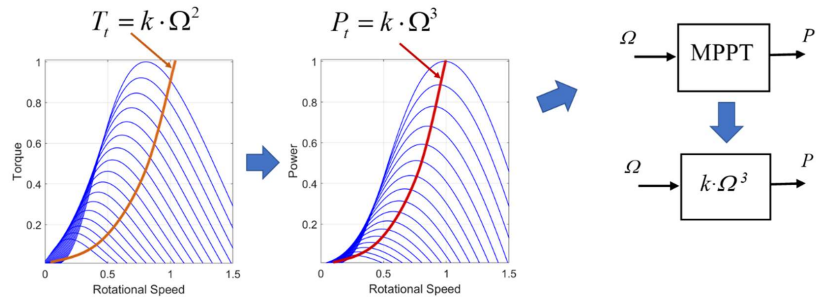


Figure 8. Electromagnetic torque T_{em} control of the generator, by controlling the power.

Thus, knowing what has been exposed before, the power generated can be mathematically expressed as:

$$P = k \cdot \Omega^3 = k \cdot (V_{dc1} \cdot k')^3 \quad (4)$$

Being k' deduced from previous equation (3):

$$\Omega \cong V_{dc1} \frac{1}{p|\psi_r|\sqrt{3}\sqrt{2}} = V_{dc1}k' \quad (5)$$

Resulting at the MPPT's power reference strategy shown in next Figure 9. Then, the power is controlled (which means to control the electromagnetic torque T_{em}) by controlling the i_{dc} with its corresponding control loop shown before in Figure 4.

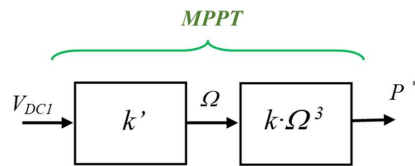


Figure 9. MPPT with power reference generation without using a speed sensor.

3.3. Only-Rectifier and Pseudo-MPPT Configurations

The power configurations analysed in this section, are simpler than the previous one. Thus, for instance Figure 10 firstly shows the generation power curve obtained with only-rectifier

configuration. This is a nearly constant rotational speed and nearly perpendicular curve, since the battery imposes a constant amplitude voltage at terminals of the generator. In practical generator designs of Small Wind Turbines, the parasitic resistance and inductance (R_s and L_s) are quite significant, therefore the power curve obtained presents a big positive slope (near 90°) as shown in Figure 10. Consequently, the generated power at each wind speed is not at the peak of the turbine's power curve, extracting at steady-state constant wind, less power than the conventional MPPT seen at the previous sub-section.

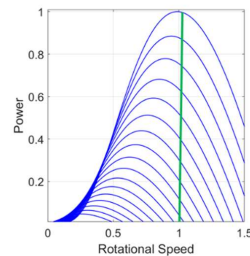
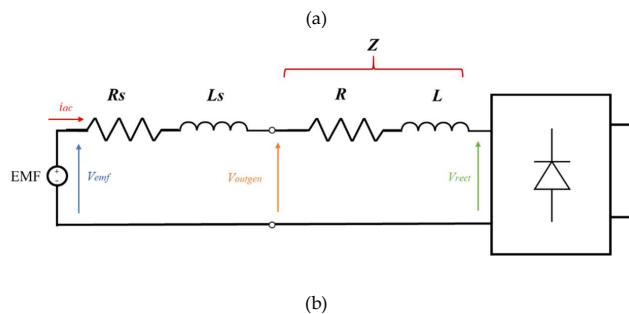


Figure 10. Generation power curve obtained with only-rectifier configuration, nearly constant rotational speed and nearly perpendicular curve. Note that in this graphical example, by choosing an appropriate DC voltage battery, a rotational speed has been chosen which nearly obtains 1 p.u. power at 1p.u. speed. This adequation is not always possible, since it depends on available system elements such as; generator's characteristics, turbine, batteries, etc.

Then, the proposed Pseudo-MPPT in [26], incorporates an impedance that in most of the cases is an inductance, but could be situations where capacitance would be more suitable. Hence, in Figure 11 (a), the simplified single phase equivalent electric circuit of the system with inductive impedance is illustrated. From this electric circuit, in Figure 11 (b), it is shown how the space vector diagram of the fundamental components of the voltage and currents are. In addition, how the MPPT power curve is moved with different L values is also shown. In general, the fundamental components of the rectifier's input voltage (imposed by voltage of the battery) and the current are nearly in phase, as shown. This fact produces that the emf voltage in which the equilibrium is reached is bigger than the rectifier's voltage. And indeed, this difference is bigger with bigger AC currents (bigger generated powers). This produces as commented before, generated power curves with positive slope near to 90° . While this slope can be made smaller, by increasing the included impedance L used as depicted in Figure 11 (b).



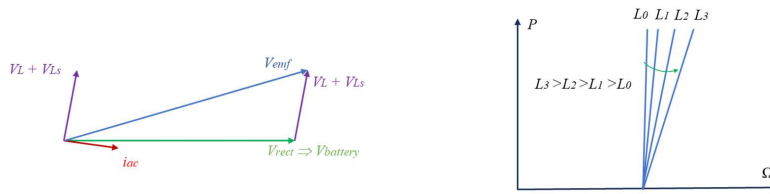


Figure 11. (a) Simplified single phase equivalent electric circuit with inductive impedance in Pseudo-MPPT concept. (b) Space vector diagram of the fundamental components of the voltage and currents and how the Pseudo-MPPT power curve is moved with different L values.

On the other hand, depending on how much the voltage of the battery is chosen, the parasitic impedances of the generator (R_s and L_s) and the wind turbine's characteristics, it could be interesting to make the slope of the generated power curve closer to positive 90° or even in some cases, make the slope bigger than 90° . This fact can be achieved as illustrated in Figure 12 (a) and (b), by including an external capacitance, which compensates the voltage drop of the parasitic inductance L_s of the generator.

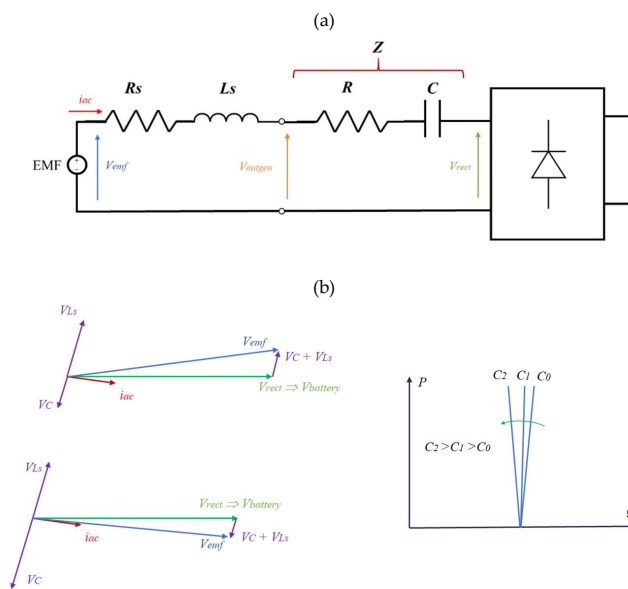


Figure 12. (a) Simplified single phase equivalent electric circuit with capacitive impedance in Pseudo-MPPT concept. (b) Space vector diagram of the fundamental components of the voltage and currents and how the Pseudo-MPPT power curve is moved with different C values.

4. Computer based Simulation Analysis

4.1. Wind Profiles at City Locations

In this subsection, several wind profiles measured at urban area of the City of Mondragon are presented. These measured wind profiles are later used in subsequent simulation analyses and are also the base for the experimental results developed in later section as well. Hence, an anemometer is placed at a terrace of the 11th building of Mondragon University at Mondragon City. The anemometer and the location of the building are shown in Figure 13. The anemometer is a WMS-21 Wind Station of Omega manufacturer whose wind measurements have been calibrated and contrasted with another portable XA1000 Lufft anemometer, to ensure accuracy. The location of the

anemometer could be a suitable place also to install a real small wind turbine for electric energy generation purposes. However, at this article, the authors could not have installed a wind turbine due to practical and administrative issues. By having and analysing the wind profiles at this location, is also a representative model of many other similar roofs and terraces of different cities, where wind profiles with similar characteristics and behaviours are expected.

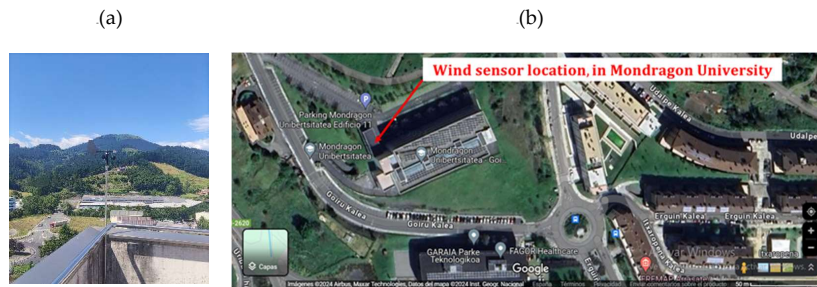


Figure 13. (a) WMS-21 Wind Station of Omega manufacturer (sample time = 1sec) located at the terrace in Mondragon University at the urban area of the City, (b) Google Map's photo showing where the anemometer has been placed for the study (place where the wind turbine can be located) at the 11th building of Mondragon University at Mondragon City.

Thus, Figure 14 shows several wind measurements with sample time of 1 second, at different moderate windy days at this city location. In addition, it must be highlighted that the authors have realized many other wind measurements with portable anemometer XA1000 Lufft, at different locations of this city and other cities, seeing that the wind profiles are always very similar. Thus, it can be noticed that the wind never is constant at least at these type of city locations. The wind is gusty, always starting from a near zero wind speed and then increases one or more than one time, until one or several peaks are reached, to finally go down again until reaching a nearly zero wind speed again. Then, this gusty wind is repeated continuously. As can be inferred carefully analysing Figure 14, the duration of the time gusts can range from some few seconds, to several dozens of seconds. Therefore, it can be concluded that the real wind speed is continuously varying, which means that the small wind turbines placed at these locations that are affected by these winds, need to adapt their rotational speed to these continuously varying winds (see previous section), in order to maximize the power extracted from these types of winds.

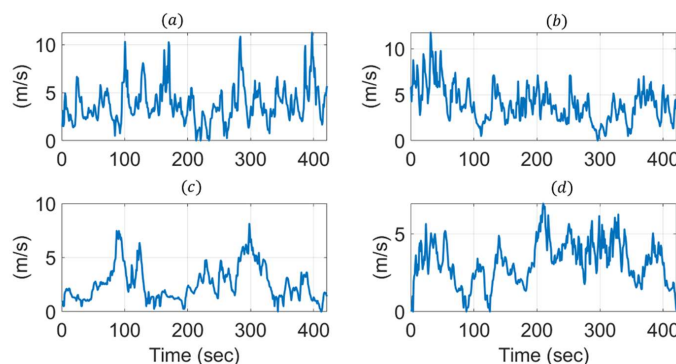


Figure 14. Wind speed measured with WMS-21 Wind Station (sample time = 1sec) at several moderate windy days in Mondragon University at the urban area of the City, (a) wind speed measurement 1, (b) wind speed measurement 2, (c) wind speed measurement 3, (d) wind speed measurement 4.

4.2. Performance Analysis with Different Inertias

In this first set of analysis, it is wanted to be understood how does the inertia of the small wind turbines affect the maximization of the energy generated. More specifically, how the gusty and continuously varying wind speed affects to the efficiency of wind turbines with different inertias. For that purpose, a fictitious and idealized wind turbine will be used, with $C_p(\lambda)$ curve shown in Figure 15 (a). It represents an averaged $C_p(\lambda)$ curve of the wind turbine that later is used at the experimental analysis, i.e., the Ayanz Wind Turbine based on Screw Blades. Note that this type of wind turbines presents a quite flat range at the higher values of the C_p curve, in the proximity of the optimum λ values where the maximum C_p is obtained.

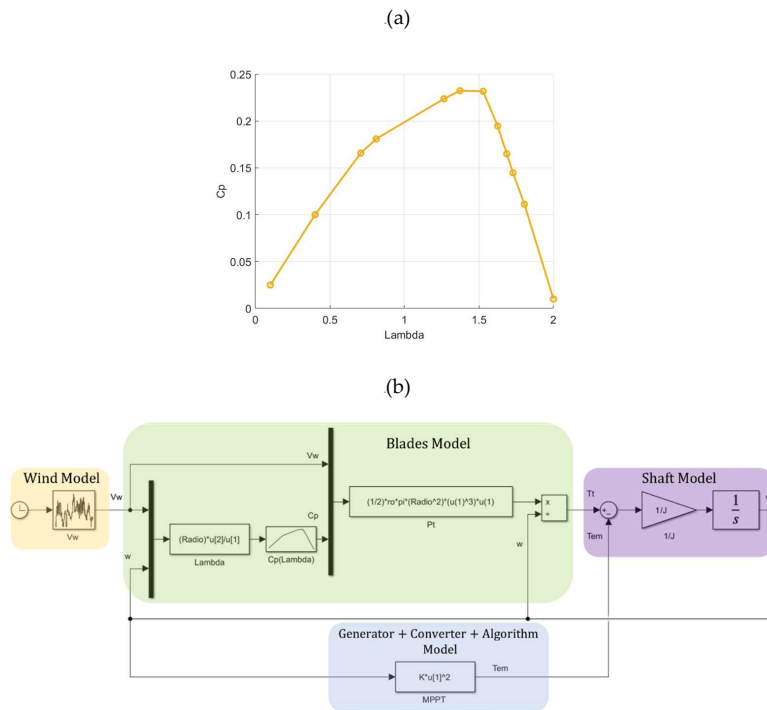


Figure 15. (a) $C_p(\lambda)$ curve of the Ayanz Wind Turbine based on Screw Blades used for the first set of simulations analyses. (b) Block diagram of the Matlab-Simulink model to perform an idealized MPPT operation of wind turbine with different inertias.

Then, Figure 15 (b) shows the block diagram of the Matlab-Simulink model employed to perform an idealized MPPT operation of wind turbine with different inertias. As can be noticed, a wind speed pattern excites the wind turbine modelled by means of the $C_p(\lambda)$ curve. This idealized model provides the torque produced by the wind turbine T_t .

Then, the idealized MPPT explained in section 3 generates the electromagnetic torque T_{em} produced by the generator-converter-algorithm. Finally, both torques interact at the rotational shaft of the turbine, modelled by a simple inertia J . This inertia, represents the sum of the shaft and generator and the dominant inertia of the wind turbine's screw blades. This idealized wind turbine model has been used in this analysis to decouple or avoid possible dynamic delays produced by realistic models of the generator, converter and control algorithm. By this approach, the MPPT's equation $T = k \cdot \Omega^2$ instantaneously provides the required electromagnetic torque (with no dynamic delay) to produce the maximization of the generated power, i.e., to produce the MPPT. In this way,

the affection of the inertia to the MPPT can be studied, decoupled from other turbine's characteristics or parameters.

Note that it could be possible to use more realistic wind model, or even more complex blades' and shaft's models than one depicted in Figure 15 (b), such as for instance incorporating stratifications phenomena, damping mechanical behaviours and others [33,34], however for simplicity purposes, these simple and very idealized models have been adopted which is enough to understand the effect of the inertia.

Hence, next Figures 16–18, show the performance of the Ayanz Wind Turbine with on Screw Blades with idealized Indirect MPPT control and different three inertia values; $J = 0.03\text{kgm}^2$, $J = 0.15\text{kgm}^2$ and $J = 0.75\text{kgm}^2$. Using the same Wind speed profile in all the cases, the obtained T_t and T_{em} performances, rotational speed, generated power, C_p and energy generated are shown. The different inertia simulated produces a different performance at the three tests. At the first one in Figure 16, with very small inertia of the wind turbine, the idealized indirect MPPT control is able to follow quickly the gusts of the wind profile studied, operating at optimum rotational speed during all the experiment and therefore, always producing the maximum achievable power at each wind speed and every instant. Therefore, during all the time the turbine operates at maximum C_p value of 0.23, with only exceptions at wind speeds zero or very near to zero (at these moments the achievable power from wind is zero). Under these circumstances the obtained energy is the maximum available from this wind speed profile which is 1212.65J.

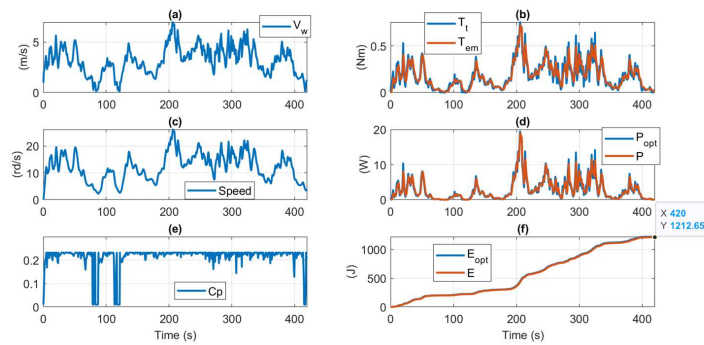


Figure 16. Performance of the Ayanz Wind Turbine based on Screw Blades with idealized Indirect MPPT control and inertia of $J = 0.03\text{kgm}^2$. (a) Wind speed profile, (b) T_t and T_{em} performances, (c) achieved rotational speed by the idealized MPPT control, (d) Optimal power with a fictitious turbine with zero inertia (P_{opt}) and actual power generated, (e) Behaviour of C_p during the test, (f) energy generated at the 420seconds test.

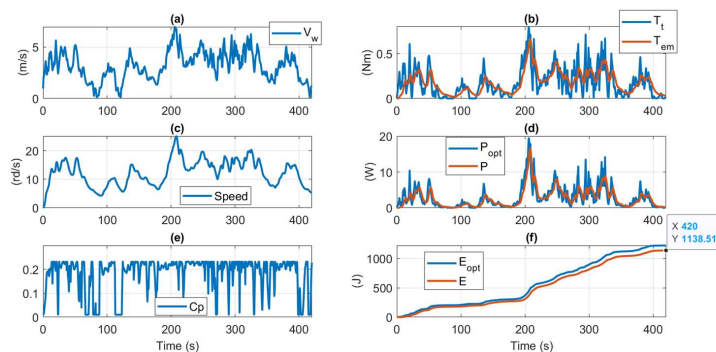


Figure 17. Performance of the Ayanz Wind Turbine based on Screw Blades with idealized Indirect MPPT control and inertia of $J = 0.15\text{kgm}^2$. (a) Wind speed profile, (b) T_t and T_{em} performances, (c)

achieved rotational speed by the idealized MPPT control, (d) Optimal power with a fictitious turbine with zero inertia (P_{opt}) and actual power generated, (e) Behavior of C_p during the test, (f) energy generated at the 420seconds test. . \

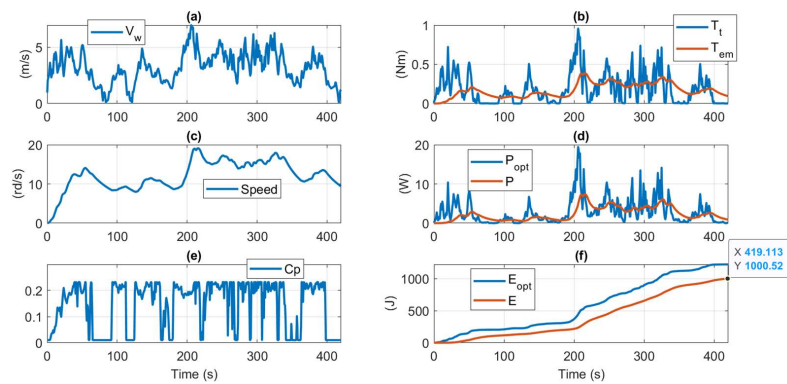


Figure 18. Performance of the Ayanz Wind Turbine based on Screw Blades with idealized Indirect MPPT control and inertia of $J = 0.75\text{kgm}^2$. (a) Wind speed profile, (b) T_t and T_{em} performances, (c) achieved rotational speed by the idealized MPPT control, (d) Optimal power with a fictitious turbine with zero inertia (P_{opt}) and actual power generated, (e) Behaviour of C_p during the test, (f) energy generated at the 420seconds test.

Then at the second experiment shown in Figure 17, with an inertia of $J = 0.15\text{kgm}^2$ which is 5 times bigger than the previous case, the idealized MPPT control is not able to follow the wind speed profile. The rotational speed now cannot evolve so quickly as before, losing part of the available power from the wind as can be noticed in Figure 17-(d). This fact produces that during the test, the turbine operates less time in the neighbourhood of the maximum C_p , producing less energy.

Then in the third experiment shown in Figure 18 with an inertia of $J = 0.75\text{kgm}^2$ which is again 5 times bigger than the previous case, the idealized MPPT still produces less energy, since the bigger inertia does not enable the wind turbine to follow the required rotational speed for maximizing energy. As summarized in Table 2, at second experiment 94% of the achievable energy is obtained while at third experiment, the energy obtained is further reduced up to 82.5%.

Table 2. Energy generated with wind speed profile of 420sec, same ideal wind turbine and same wind speed profiles at different inertias.

| Energy generated during the ideal wind turbine test | | |
|---|----------|-------------|
| Inertia | Energy | % of Energy |
| $J = 0.03\text{kgm}^2$ | 1212.65J | 100% |
| $J = 0.15\text{kgm}^2$ | 1138.52J | 94% |
| $J = 0.75\text{kgm}^2$ | 1000.52J | 82.5% |

This tendency clearly demonstrates that the inertia of the wind turbine is a key parameter when designing small wind turbines to be placed at urban area of city locations, where the wind speed varies quite quickly. Therefore, if the generated energy is wanted to be maximized, wind turbine morphologies whose equivalent inertias are ‘small’ are more suitable to be used. And if it is possible, light materials that further minimize the inertia of the blades would be the best option, but as always, finding the equilibrium with the mechanical robustness.

4.3. Performance Analysis with Different MPPT Control Dynamics

In this sub-section, the effect of the closed loop control dynamics of the MPPT is analysed, on the energy production of the wind turbine. In this case, the employed wind turbine model incorporates the PM generator, the rectifier and the DC-DC converter, together with a realistic MPPT control as presented in Figure 19. The entire model has been implemented in Matlab-Simulink. As can be noticed, compared with the block diagram presented in Figure 4 of previous section, in this case, a low pass filter has been included at the input of the current reference i_{dc} . This is necessary to guarantee the stability of the closed loop system performance. Note that the oscillations or ripples that could present V_{dc1} , if they are not filtered, can be feedbacked to the current loop, increasing them over and over again to V_{dc1} until stability is lost. In order to avoid this undesired situation, a typical and easy solution is to include a low pass filter as illustrated in Figure 19. The value for the time constant τ , in general is simply tuned by try and error, since it depends on the electric parameters characteristics as well as the tendency to produce torque and speed oscillations of the specific morphology of wind turbine studied. Other filter or smoothing philosophies could be adopted, but in this case for simplicity, a simple first order filter has been used.

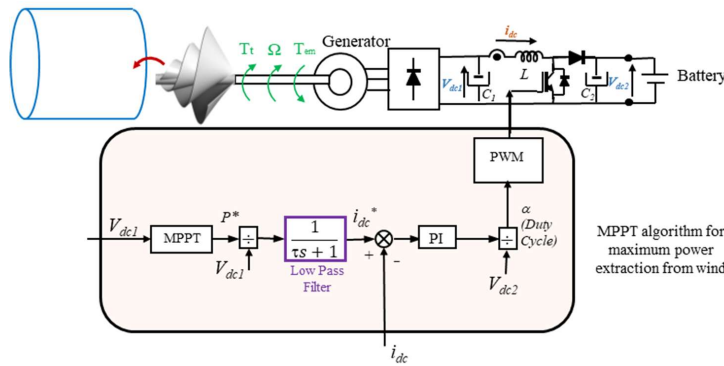


Figure 19. Indirect Speed Control MPPT including a low pass filter to ensure stability of the system.

Hence, Figures 20 and 21, show the performance of the Ayanz Wind Turbine with Screw Blades with Indirect MPPT control and different time constants (τ), of low pass filter for smoothing V_{dc1} oscillations. In this case, a realistic value of $J = 0.15 \text{ kgm}^2$ inertia has been adopted.

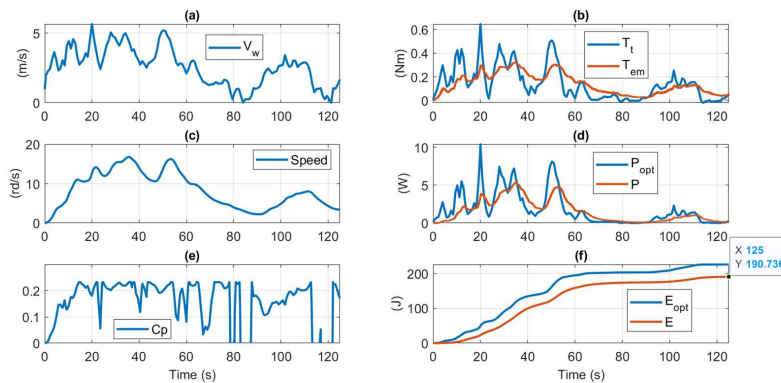


Figure 20. Performance of the Ayanz Wind Turbine based on Screw Blades with Indirect MPPT control and $\tau=1\text{sec}$ at low pass filter for smoothing V_{dc1} oscillations ($J = 0.15 \text{ kgm}^2$, $V_{\text{battery}}=48\text{V}$). (a) Wind speed profile, (b) T_t and T_{em} performances, (c) achieved rotational speed by the idealized MPPT control, (d) Optimal power with a

fictitious turbine with zero inertia (P_{opt}) and actual power generated, (e) Behavior of C_p during the test, (f) energy generated at the 125seconds test.

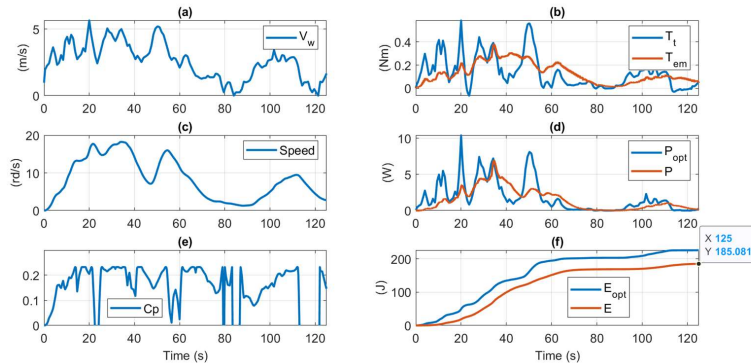


Figure 21. Performance of the Ayanz Wind Turbine based on Screw Blades with Indirect MPPT control and $\tau=6\text{sec}$ at low pass filter for smoothing V_{dcl} oscillations ($J = 0.15\text{kgm}^2$, $V_{battery}=48\text{V}$). (a) Wind speed profile, (b) T_t and T_{gm} performances, (c) achieved rotational speed by the idealized MPPT control, (d) Optimal power with a fictitious turbine with zero inertia (P_{opt}) and actual power generated, (e) Behavior of C_p during the test, (f) energy generated at the 125seconds test.

The wind speed profile, is the first 125seconds of the previously employed wind speed profile. In Figure 20, with a realistic $\tau=1\text{sec}$, it is seen that the energy generated at the mechanical shaft of the generator (190.7J) is below the maximum available energy at each wind speed. This happens due to the filter introduced delay, generator's dynamic delay and the inertia delay itself. However, when the quite extreme unfavourable case of $\tau=6\text{sec}$ is tested, as depicted in Figure 21, the achieved energy is further reduced to 185J (3%). This means that the closed loop control dynamic, mainly determined by this filter dynamic (because the generator's electric dynamic and the current loop dynamics are normally faster) can also slow down the turbine's performance, moving away from the maximum values of C_p and therefore, further reducing the generated energy.

4.4. Performance Analysis with Uncertainty at MPPT Curve

In this sub-section, the uncertainty of the MPPT curve is analysed into the energy production of the wind turbine. In this case, the same wind turbine model is employed as in previous sub-section, but an additional realistic fact has been considered at the control. Often, the MPPT curve $P=f(V_{dcl})$ is not so accurately known due to many reasons, being perhaps the principal one, the fact that often the wind turbine cannot be accurately characterized (not availability of wind tunnel to excite the turbine as desired, not availability of accurate wind sensors, not availability of electric power sensors, etc). Knowing this, it is not realistic to study the performance of the wind turbine assuming that an exact $P=f(V_{dcl})$ is known, which is a very common situation in many commercial wind turbines. In addition, often these scenarios operate at low-cost conditions, using not so accurate current or voltage sensors for the MPPT algorithm. Hence, considering all what is said here, the MPPT control considering uncertainties has been implemented in Matlab-Simulink as depicted in Figure 22.

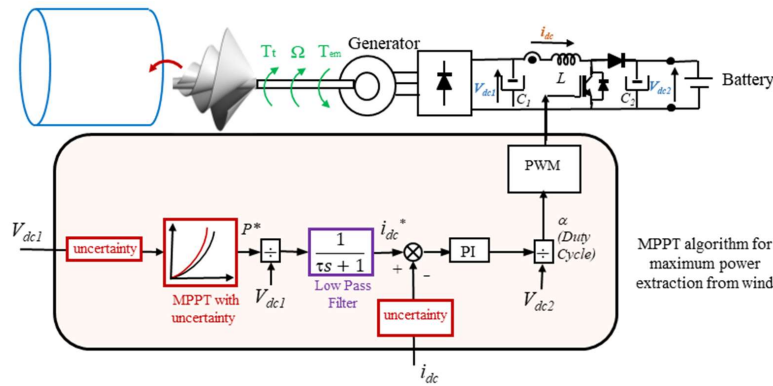


Figure 22. Indirect Speed Control MPPT including a low pass filter to ensure stability of the system and including also uncertainties at MPPT curve and current and voltage sensors.

As before carried out experiments, the low pass filter has been also left at the MPPT control algorithm while the inertia is also left to the realistic case of $J = 0.15 \text{ kgm}^2$. Hence, equivalent simulation model-based test has been performed as in the previous sub-section, with the same wind speed profile but in this case, with a realistic uncertainty at the MPPT curve of 20% (optimum constant k with an error of 20%) and error at the current and voltage sensors of 5%. The experiments' results are shown in Figure 23. Compared with the results of previous sub-section of Figure 20, it is seen that the realistic uncertainty provokes a further reduction of the generated energy from 190.7J to 182.1J (around of 5% of reduction in 125seconds of test). This important fact is not often studied, but is present in many small wind turbine designs.

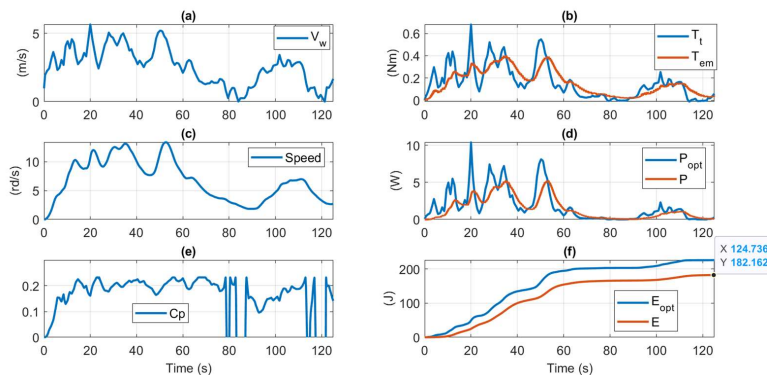


Figure 23. Performance of the Ayanz Wind Turbine based on Screw Blades with Indirect MPPT control and uncertainty at the MPPT curve of 20% (optimum constant k with an error of 20%) and error at the current and voltage sensors of 5% ($\tau=1\text{sec}$ at low pass filter, $J = 0.15 \text{ kgm}^2$, $V_{\text{battery}}=48\text{V}$). (a) Wind speed profile, (b) T_t and T_{em} performances, (c) achieved rotational speed by the idealized MPPT control, (d) Optimal power with a fictitious turbine with zero inertia (P_{opt}) and actual power generated, (e) Behavior of C_p during the test, (f) energy generated at the 125seconds test.

4.5. Performance Analysis of Pseudo-MPPT and Only Rectifier Power Conversion Systems

In this sub-section, the other two simplified power conversion topologies are analysed. In both cases, the same electric generator, rectifier and C_1 capacitance are used as in previous subsections when MPPT control was implemented. Hence, first of all, Figure 24 shows the only-rectifier performance with same wind speed profile as previous tests. A battery of 36V has been used, after

testing battery voltages of 12V, 24V and 48V and providing worse results than with 36V at this wind profile. It is seen that an energy of 178.36J is obtained in this case, which is very close to the previous experiment with MPPT (only 2% of energy reduction).

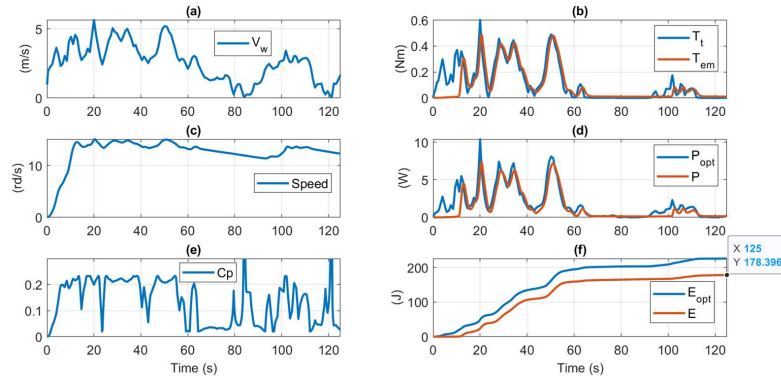


Figure 24. Performance of the Ayanz Wind Turbine based on Screw Blades with Only-rectifier power conversion system ($J = 0.15 \text{ kgm}^2$, $V_{\text{battery}} = 36 \text{ V}$). (a) Wind speed profile, (b) T_t and T_{em} performances, (c) achieved rotational speed by the idealized MPPT control, (d) Optimal power with a fictitious turbine with zero inertia (P_{opt}) and actual power generated, (e) Behaviour of C_p during the test, (f) energy generated at the 125seconds test.

Obviously in this case, the rotational speed is maintained quite constant and the variations are due to the voltage drop at the parasitic resistance and inductances of the generator ($R_s = 9.56 \Omega$, $L_s = 20.96 \text{ mH}$). Thus, it is observed that at this wind speed profile, by choosing a 36V battery, it is possible to obtain quite good energy generation results. Then, in Figure 25 the same experiment is carried out but now including and external inductance of $L = 30 \text{ mH}$ in order to perform a Pseudo-MPPT. It is seen that the achieved generated energy is slightly smaller than at the previous experiment without external L . After several trials, it has been seen that the only way of increasing the energy generated would be in this situation, by reducing the total L of the generator. As depicted in Figure 26, with the Only-Rectifier power conversion systems and a reduction of the parasitic L_s inductance of $L_s = 20.96/3 \text{ mH}$, the generated energy of the system is increased to 189J, which is a 4% of energy increase with respect to the MPPT power conversion system (Figure 23).

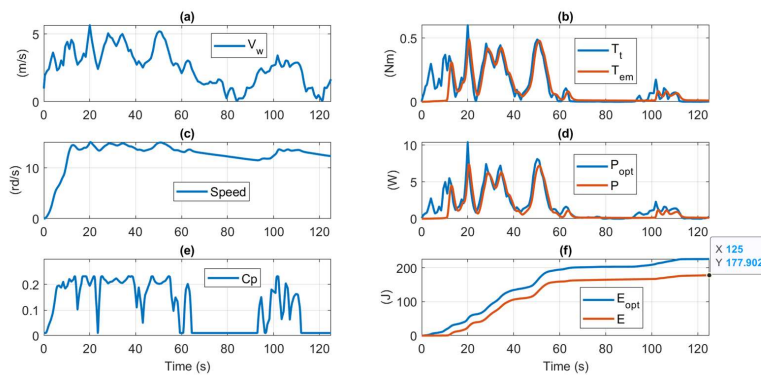


Figure 25. Performance of the Ayanz Wind Turbine based on Screw Blades with Pseudo-MPPT power conversion system and external $L = 30 \text{ mH}$ ($J = 0.15 \text{ kgm}^2$, $V_{\text{battery}} = 36 \text{ V}$). (a) Wind speed profile, (b) T_t and T_{em} performances, (c) achieved rotational speed by the idealized MPPT control, (d) Optimal power with a fictitious turbine with

zero inertia (P_{opt}) and actual power generated, (e) Behavior of C_p during the test, (f) energy generated at the 125seconds test.

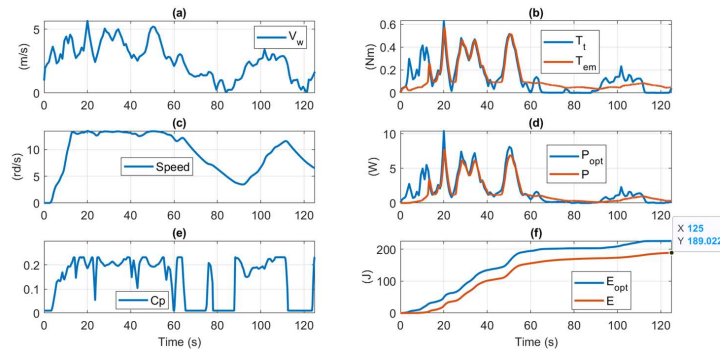


Figure 26. Performance of the Ayanz Wind Turbine based on Screw Blades with Only-rectifier power conversion system and generator's inductance of L_s divided by 3 ($J = 0.15 \text{ kgm}^2$, $V_{\text{battery}} = 36 \text{ V}$). (a) Wind speed profile, (b) T_t and T_{em} performances, (c) achieved rotational speed by the idealized MPPT control, (d) Optimal power with a fictitious turbine with zero inertia (P_{opt}) and actual power generated, (e) Behavior of C_p during the test, (f) energy generated at the 125seconds test.

In a real case, it would represent a change in the generator with a had-oc design, trying to reduce the parasitic inductance, whenever is possible and practical to be achieved. It has to be highlighted that the only-rectifier and Pseudo-MPPT conversion systems, will have fewer electric losses due to the omission of the DC-DC converter and the microprocessor that could range around of 1.5W using standard electric components. Note that in all the cases, the power and energy that is being evaluated is at the mechanical shaft of the turbine. In addition, the MPPT system, as drawbacks compared with the other two simpler versions, needs to tune control parameters and quite accurately known the turbine aerodynamic performance (k constant).

4.6. Performance Analysis of a Wind Turbine with Shorter Range of Values with C_{pmax} (Peaked C_p Curve)

In this last sub-section, the previously analysed power conversion configurations are tested in a fictitious wind turbine with shorter range of values with C_{pmax} . Thus, as depicted in Figure 27, the new with turbine to be studied presents a thinner range of lambda values where the C_p values are close to the C_{pmax} . This again possible and realistic situation depending on the morphology of the wind turbine, will require a more precise and quicker MPPT control to operate at C_{pmax} values, since a short rotational speed deviation from the optimum, will imply a higher loss of efficiency than the previously studied wind turbine.

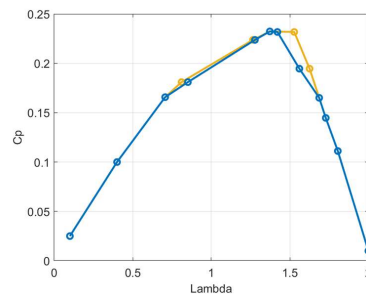


Figure 27. $C_p(\lambda)$ curve of the Ayanz Wind Turbine based on Screw Blades used for the second set of simulations analyses (Blue: new C_p curve, Yellow: previous tests' C_p curve) with a shorter range of values with C_{pmax} .

Hence, Figures 28–30 present the same tests as performed in previous subsections, with the same wind profiles of 125seconds of duration and with the three proposed power conversion systems. In Figure 28, it can be noticed that with this more peaked $C_p(\lambda)$ curve, the Indirect MPPT generates less energy (178.5J) than with previous C_p curve (182.1J) in Figure 23).

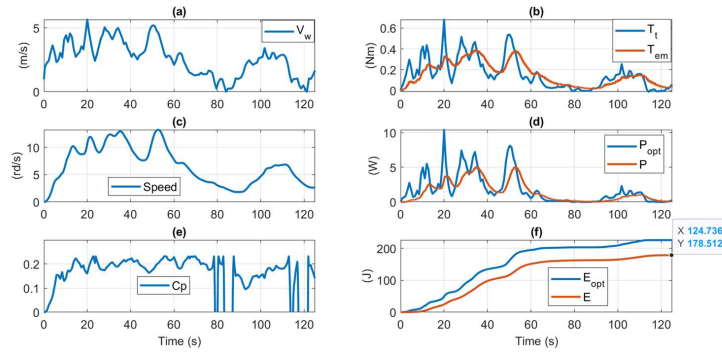


Figure 28. Performance of the Ayanz Wind Turbine based on Screw Blades with Indirect MPPT control and second more peaked curve of $C_p=f(\lambda)$ (uncertainty at the MPPT curve of 20%, error at the current and voltage sensors of 5%, $\tau=1\text{sec}$ at low pass filter, $J = 0.15\text{kgm}^2$, $V_{\text{battery}}=48\text{V}$). (a) Wind speed profile, (b) T_t and T_{em} performances, (c) achieved rotational speed by the idealized MPPT control, (d) Optimal power with a fictitious turbine with zero inertia (P_{opt}) and actual power generated, (e) Behavior of C_p during the test, (f) energy generated at the 125seconds test.

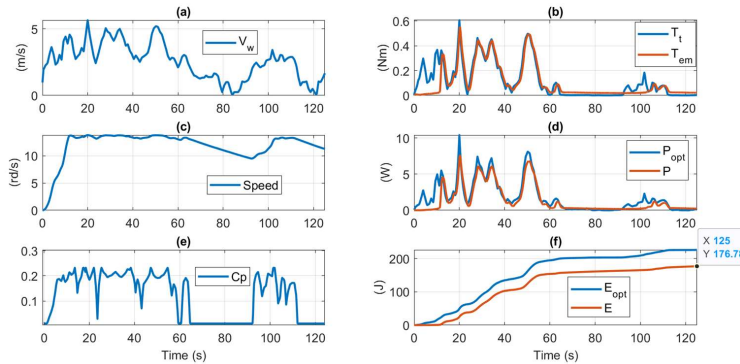


Figure 29. Performance of the Ayanz Wind Turbine based on Screw Blades with Only-Rectifier power conversion system and second more peaked curve of $C_p=f(\lambda)$ ($J = 0.15\text{kgm}^2$, $V_{\text{battery}}=36\text{V}$). (a) Wind speed profile, (b) T_t and T_{em} performances, (c) achieved rotational speed by the idealized MPPT control, (d) Optimal power with a fictitious turbine with zero inertia (P_{opt}) and actual power generated, (e) Behavior of C_p during the test, (f) energy generated at the 125seconds test.

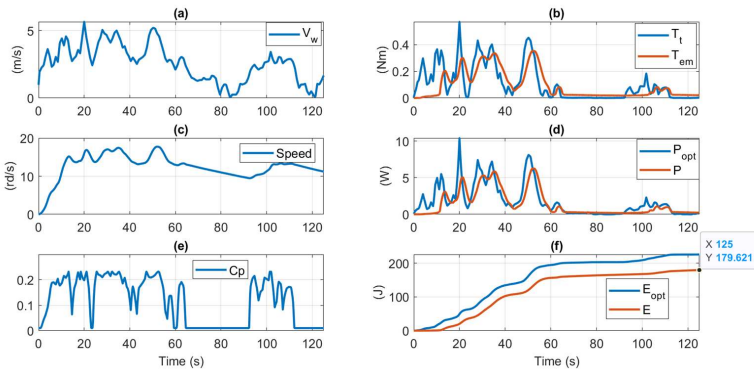


Figure 30. Performance of the Ayanz Wind Turbine based on Screw Blades with Pseudo-MPPT power conversion system (series external C=0.1mF at three phases) and second more peaked curve of $C_p=f(\lambda)$ ($J = 0.15\text{kgm}^2$, $V_{\text{battery}}=36\text{V}$). (a) Wind speed profile, (b) T_l and T_{em} performances, (c) achieved rotational speed by the idealized MPPT control, (d) Optimal power with a fictitious turbine with zero inertia (P_{opt}) and actual power generated, (e) Behaviour of C_p during the test, (f) energy generated at the 125seconds test.

As commented before, this is due to the fact that the MPPT control accompanied with its uncertainties and delays in responses, is not able to avoid a certain deviation from the optimum rotational speed that finally generates a bigger deviation from the C_p maximum value. The difference is nearly 2%, which is not so high, but gives an idea of how the characteristics of the wind turbine, combined with the control parametrization and the wind profiles, can produce certain produced energy variations.

Then, in Figure 29, performance of the Ayanz Wind Turbine based on Screw Blades with Only-Rectifier power conversion system and second more peaked curve of $C_p=f(\lambda)$ is shown. Again, there are not big differences and the generated energy is around 176.8J, compared with previous wind turbine (178.4J) in Figure 24).

Finally, several simulations have been carried out with the Pseudo-MPPT concept with this more peaked C_p wind turbine. It has been noticed that with external inductances, it has not been possible to improve the generated energy. However, it has been observed that including series capacitive impedances, the improvement has been possible. Thus, Figure 30 shows the pseudo-MPPT power conversion system with series external $C=0.1\text{mF}$ at the three phases and second more peaked curve of $C_p=f(\lambda)$. It can be observed that the generated energy now is 179.6J, which is the highest obtained energy with this more peaked C_p curve. Again, the differences are not significative, but gives an idea that the MPPT is not always the best option for maximizing the generated energy. Wind speed conditions, together with key characteristics of the wind turbine (inertia, shape of the C_p curve), can provoke that any of the three studied power conversion configurations could be the one that maximizes the generated power. Consequently, often it could be possible that we can avoid the utilization of complex MPPT controls and go for more simpler, cheaper and with less power losses configurations such as the Pseudo-MPPT or even the Only-Rectifier version.

Finally, Table 3 summarizes the last results obtained at this simulation-based analysis.

Table 3. Summary of the results obtained at the comparison between power conversion system configurations.

| | Energy generated with first $C_p(\lambda)$ | Energy generated with second $C_p(\lambda)$ (peaked curve) |
|--|---|--|
| MPPT | | |
| ($J = 0.15\text{kgm}^2$, uncertainty at MPPT curve: 20%, error at I and V sensors; 5%, $\tau=1\text{sec}$ at LP filter, $J = 0.15\text{kgm}^2$) | 182.1 J | 178.5 J |

5.1. Wind Maker

(a)



(b)

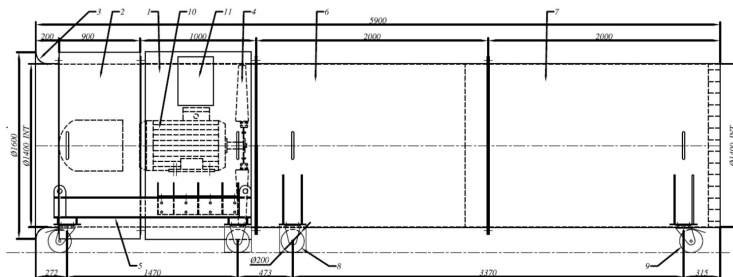


Figure 31. (a) Photo of the Wind maker used for the experimental validation at laboratories of Mondragon university, (b) characteristics of the wind maker [26].

5.2. Real Wind Turbine Used at the Experimental Validation: The Ayanz Wind Turbine based on Screw Blades

The wind turbine used at the experimental tests is the Ayanz Wind Turbine based on Screw Blades previously shown in Figure 1. The aerodynamic characterization of this commercially available turbine was published in a previous article; [26]. Since the wind maker produces a wind speed not equal in the whole area of the circumference outlet, in order to precisely know what wind is affecting the wind turbine, a mean of several wind measurements is carried out. By using an XA1000 Lufft portable wind speed sensor, it is placed at different input points of the turbine, which are marked in red in Figure 32-(a). For each point and frequency setpoint (wind speed setpoint), a measurement was taken in a time window of at least 25 seconds and the velocities obtained during this interval were averaged. Figure 32-(b) shows the results obtained and the averaged wind speed considered in blue, which is the mean of the red point measurements.

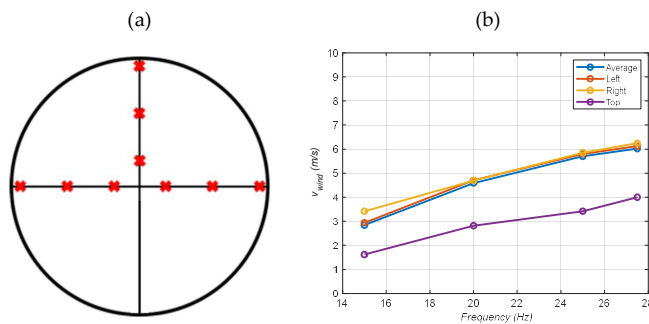


Figure 32. (a) Wind measurement points (in red) taken just in the front area of the turbine, (b) Wind measurements at the wind turbine's input with tube (obtained and first published in [26]).

After that, once the wind speed measurements are obtained, experimental characterization of the wind turbine is carried out. The wind turbine is excited with the wind maker and the power at an external passive load located at the generators' output is measured. Then, the power curves of the wind turbine are obtained which are shown in Figure 33. For more information about the experimental characterization the reader is referred to [26].

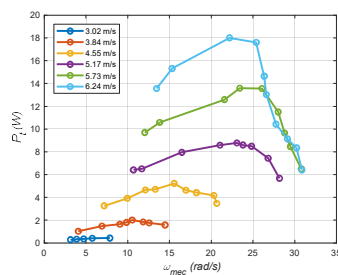


Figure 33. Power curves of the Ayanz Wind Turbine based on Screw Blades (obtained and first published in [26]).

Once having the power curves of the wind turbine characterized, Figure 34 (a) and (b) show the Power curves of the Ayanz Wind Turbine based on Screw Blades. First, in Figure 34-(a) curves with ideal MPPT and Only-Rectifier configurations at different batteries voltages (24V are 2 batteries in series while 40V are 3 batteries in series) are shown, while in Figure 34-(b) ideal MPPT, only-Rectifier and Pseudo-MPPT configurations at 40V of battery voltage are provided. It has to be remarked that these curves are obtained with the wind maker producing a constant wind speed, which means that

are curves at steady-state operation conditions. However, as has been shown in previous section, the wind at city locations is not constant, since it varies in gusty shapes.

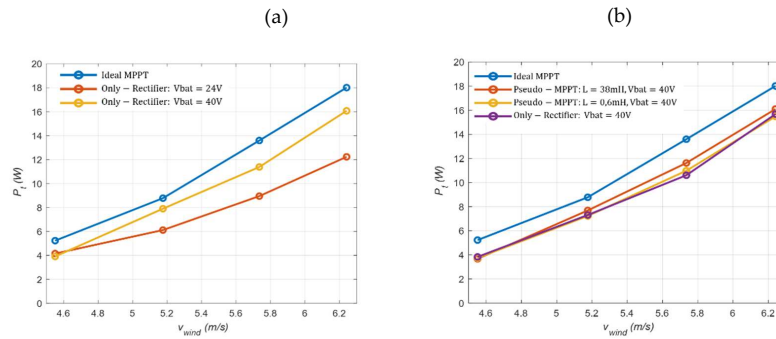


Figure 34. Power curves of the Ayanz Wind Turbine based on Screw Blades at constant wind speeds (obtained and first published in [26]). (a) Ideal MPPT and Only-Rectifier configurations at different batteries voltages (24V are 2 batteries in series while 40V are 3 batteries in series). (b) Ideal MPPT, Only-Rectifier and Pseudo-MPPT configurations at 40V of battery voltage.

5.3. Wind Profiles Used at the Experimental Tests

Once the wind turbine is characterized, the next step is to test it at realistic variable wind speeds typical from city locations. In Figure 35, a graphical simplified pattern identification of wind speed measured at the urban area of the Mondragon City is depicted. As noticed, the complex and very variable wind profile, can be somehow simplified to 'ramp based' wind profiles superposed in the figure with red colour.

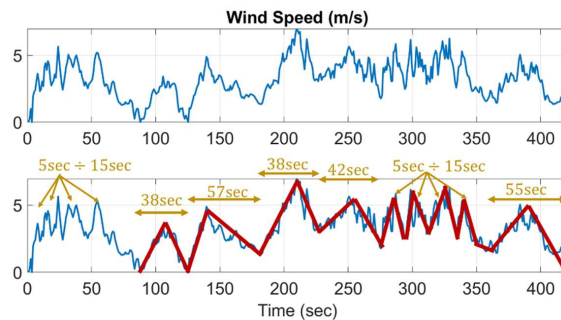


Figure 35. Simplified pattern identification of wind speed measured with XA1000 Lufft anemometer (sample time = 1sec) at a moderate windy day in Mondragon University at the urban area of the city (same wind profile used in previous simulation-based analysis section).

The fastest variations of wind speed, wind turbines are not able to follow (at least with these dimensions), due to their natural intrinsic inertia. Therefore, at the laboratory tests with the wind maker, the fastest wind variations will not be reproduced and only 'ramp-based' wind speed variations would be implemented. In addition, it has to be highlighted that the wind maker does not have capacity to reproduce very fast wind speed variations, due to its dynamic response capacity limitation. So even if wanted, it would be impossible to reproduce faithfully and accurately the quick varying wind speed profile of Figure 35.

Hence, Figure 36-(a) in a simplified manner, show that although in reality the typical pattern of wind gusts (neglected the fastest super-posed wind variations), may present different increasing and decreasing slopes and different also starting and ending wind speeds, for simplicity, this fact will be neglected and equal initial-end slopes and winds will be considered, as depicted in Figure 36-(b).

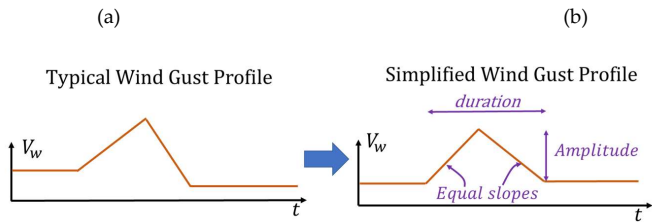


Figure 36. Simplified wind gust profile used at laboratory tests in subsequent sections.

Consequently, the experimental test will be restricted to study the behaviour of wind turbines to ‘ramp based’ wind patterns and to measure the power end energy generated by the wind turbine with different power conversion system configurations as graphically illustrated in Figure 37.

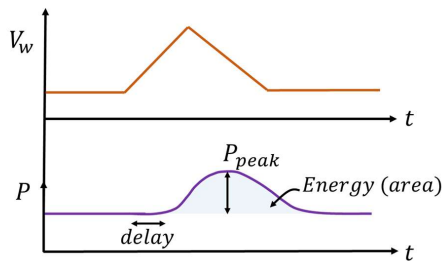
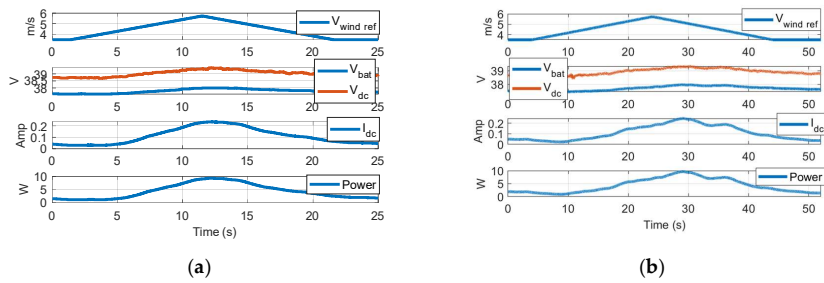


Figure 37. Simplified wind gust profile used at the experimental tests and obtained power and energy with the wind turbine.

5.4. Performance at Variable Wind Speed: Simplified ‘Ramp-Based’ Wind Gust Profiles

With the real wind profiles determined, the next step is to test the performance of these with the real Ayanz wind turbine and the only rectifier, the pseudo MPPT and the MPPT. Each of these topologies are tested in four different scenarios, specifically, to four different wind gusts. To reproduce the ‘ramp-based’ wind gust profiles, Matlab’s Simulink blocks has been used and the four wind gust profiles have been of 20 seconds, 40 seconds, 60 seconds and 80 seconds.



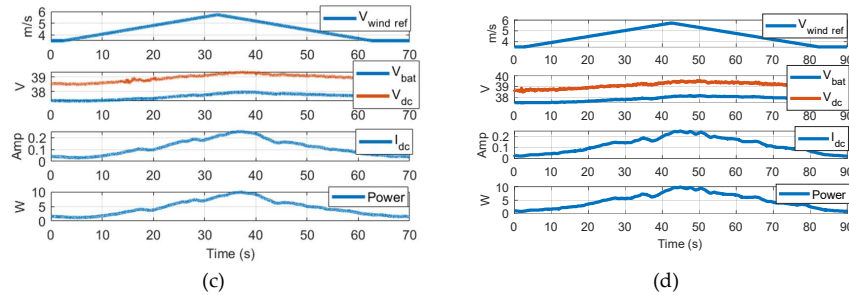


Figure 38. Performance of the Ayanz Wind Turbine with screw blades at variable wind speed tests, with only rectifier power conversion system. (a) 10sec + 10sec wind gust, (b) 20sec + 20sec wind gust, (c) 30sec + 30sec wind gust, (d) 40sec + 40sec wind gust.

Likewise, the gusts are simetrical which means that half of the gust ascends to the maximum the the other half descends from maximum to minimum. It is important to mention that during all the tests, the minimum and the maximum wind values have not been changed, the only ones changed have been the gust times. In order for the test to be the most accurate, the maximum and minimum values have been defined taking into account all the data mentioned in section 5.3, being the minimum wind reference of 3.51m/s and the maximum wind reference of 5.73m/s. It is important to mention that for all the test developed during this section, the Ayanz was already spinning at 3.51m/s. Hence, as depicted in Figure 38, the first analysed case has been the one related to the only rectifier. In all four cases, it can be seen that the power peak is given after de reference wind speed peak happens, meaning that a delay happens between both. This means that in reality, the system behaves as it should (compared to Figure 37). Other important factor that can be seen is that the voltage on the batteries is lower than the one in rectified side, this happens due to the voltage drops that occur through the diodes of the converter mainly.

Then, the results presented in Figure 39 are the ones related to the Pseudo-MPPT. The inductance used for this has been of 38mH and has been placed before the rectifier in the three phases. As in the previous case, a delay appears between the wind reference maximum point and the peak power point, indicating positive results.

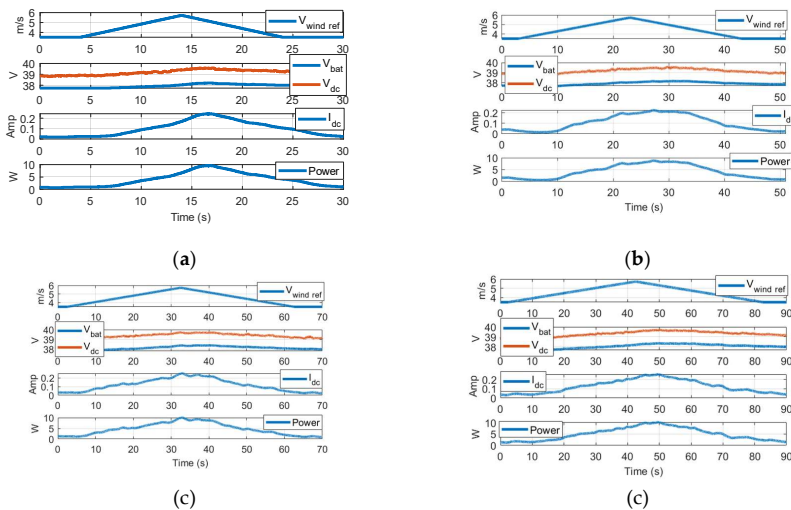


Figure 39. Performance of the Ayanz Wind Turbine with screw blades at variable wind speed tests, with Pseudo-MPPT power conversion system with L=38mH. (a) 10sec + 10sec wind gust, (b) 20sec + 20sec wind gust, (c) 30sec + 30sec wind gust, (d) 40sec + 40sec wind gust.

Figure 40 shows the results related to the MPPT. In this case, it can be seen that V_{dc1} is no longer constant and varies throughout the gust. This happens due to the MPPT system, which works based on the voltage that is measured and produces the power reference, affecting all the controlled system. As in the previous two cases, the mentioned delay appears, proving the favourable results. Moreover, for the MPPT case there is another important parameter that appear in the figure, i.e. the duty cycle. The behaviour of the duty cycle is based on the battery and V_{dc1} voltages. As it can be seen in the figure, as long as the V_{dc1} increases and approximates the V_{bat} voltage, the duty cycle becomes smaller. This happens because the MPPT system works with a boost topology.

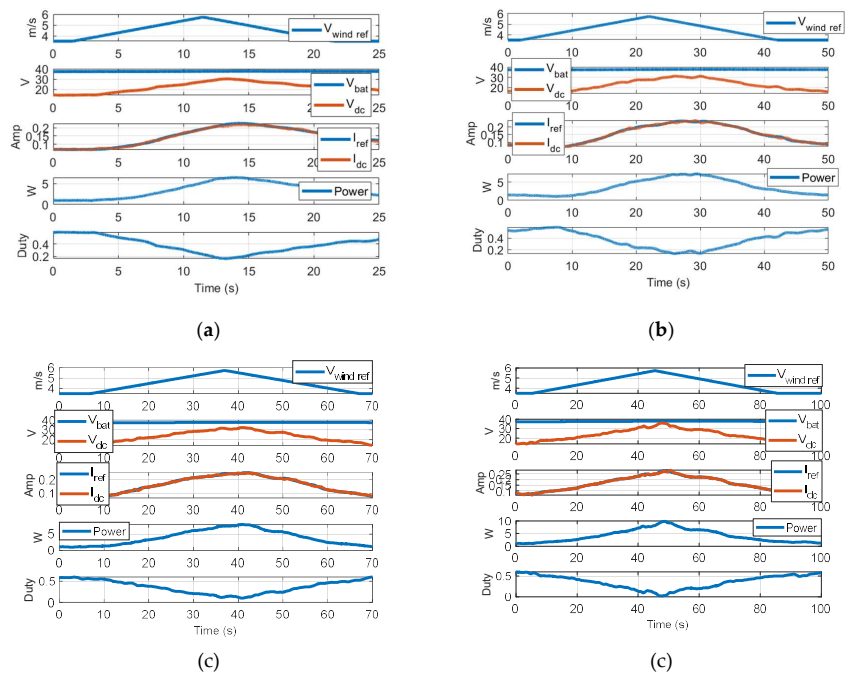


Figure 40. Performance of the Ayaz Wind Turbine with screw blades at variable wind speed tests, with MPPT. (a) 10sec + 10sec wind gust, (b) 20sec + 20sec wind gust, (c) 30sec + 30sec wind gust, (d) 40sec + 40sec wind gust.

As the 3 scenarios have depicted, the next steps is to analyse which of them generates the biggest power peak and the most energy for the four wind gusts. All this information can be seen in Table 4.

| Wind speed profile | Energy and peak of power generated during the test | | |
|-------------------------|--|--|--|
| | Only rectifier | Pseudo-MPPT | MPPT |
| 10sec + 10sec wind gust | E= 6.295 J P _{peak} = 9.3 W | E= 8.112 J P _{peak} = 9.59 W | E= 6.13 J P _{peak} = 6.48 W |
| 20sec + 20sec wind gust | E= 12.814 J P _{peak} = 9.62 W | E= 14.88 J P _{peak} = 8.83 W | E=12.46 J P _{peak} = 7.31 W |
| 30sec + 30sec wind gust | E= 22.204 J P _{peak} = 9.83 W | E= 23.246 J P _{peak} = 10 W | E= 19.96 J P _{peak} = 8 W |
| 40sec + 40sec wind gust | E= 30.874 J P _{peak} = 9.91 W | E= 31.12 J P _{peak} = 10.1 W | E= 29.47 J P _{peak} = 9.87 W |

For the scenario presented, the best power conversion system is the Pseudo-MPPT, it has the biggest power peaks and the most energy for the four wind gusts. Then, the only rectifier topology has quite good numbers too. Finally, the MPPT system is the worst of the three, especially in the fast wind gusts (referring to maximum power values). This may happen since the control slows the system and does not have enough time to follow the wind gust correctly, this can be seen in the last wind gust where the MPPT approximates to the other two topologies. Nevertheless, the energy obtained by the MPPT system is quite equal to the other two. Looking to the table in a more general way, it can be said that despite the difference in both analysed values, it is not a very big difference between all of them, specially between the only rectifier and the Pseudo-MPPT power conversion system.

5.5. Performance at Variable Wind Speed and Turbine Initially Wrongly Oriented to the Wind's Direction

It is important to remark that the wind has not the same direction always in City locations where are many obstacles as depicted in Figure 41. Normally most the tests found in specialized literature, tend to assume that the direction of the wind is constant. However, in reality in cities the turbulent winds tend to change direction in quite a fast way during some few seconds. This fact ensures the importance of testing the Ayanz wind turbine along the MPPT conversion system with different initial orientations and different wind gusts. Making this test, the adaptability and reliability of the Ayanz with turbine to different orientated gusts is evaluated. The tests are not intended to describe exactly the real winds, since this would be very difficult to be reproduced at laboratory. Instead, it is wanted to obtain a rough and basic idea of how much energy is lost in a simplified wind direction's variation at the studied Ayanz wind turbine.

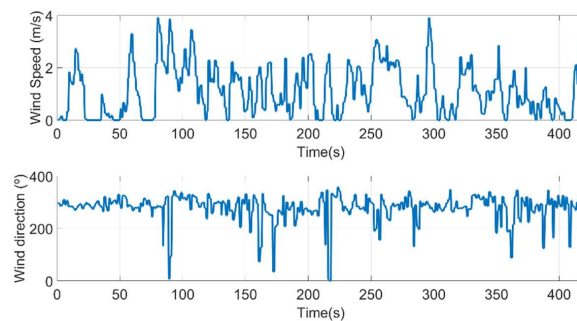


Figure 41. Wind speed and wind speed direction in a low-moderate windy day (Anemometer: WMS-21 Wind Station of Omega manufacturer, with sample time=0.5sec). During the measurements, the wind's direction is dominantly around 300° (coming from North-West) but during some few seconds intervals, the direction changes quickly dozens of degrees.

Figure 42 shows the results obtained for de orientation changing tests. Two wind gusts have been used for this test: one of 20 seconds (10seconds increasing wind and 10 seconds decreasing wind) and other of 100 seconds (50seconds increasing and 50 seconds decreasing). For each wind gust two initial orientations have been used: 15° wrongly orientated and 45° wrongly orientated. For a more realistic definition of the test, before starting with the test, the Ayanz turbine was already rotating and just when the ramp wind started, the Ayanz turbine was disorientated the defined degrees for the test.

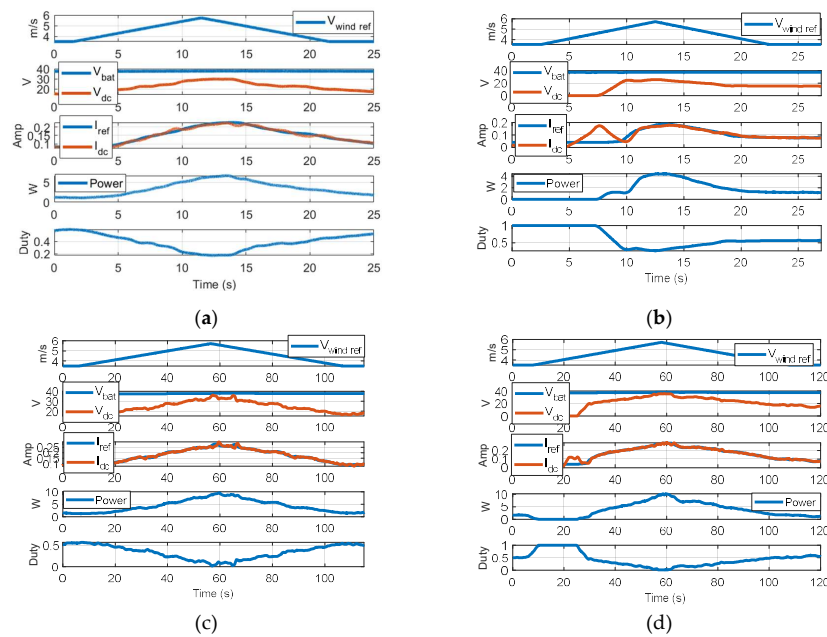


Figure 42. Performance of the Ayanz Wind Turbine with screw blades at variable wind speed tests, with MPPT power conversion system and turbine initially wrongly oriented. (a) 10sec + 10sec wind gust and turbine initially 15° wrongly oriented, (b) 10sec + 10sec wind gust and turbine initially 45° wrongly oriented, (c) 50sec + 50sec wind gust and turbine initially 15° wrongly oriented, (d) 50sec + 0sec wind gust and turbine initially 45° wrongly oriented.

In Figure 42-(a) and 42-(b), the results of the 20 second test can be seen. The orientation time for this two is of 4 seconds. The difference between both is that for the 42-(a) case, the Ayanz turbine does not stop rotating because of some part of the gust indeed affects the blades. While for the 42-(b), as the disorientation angle is much bigger, the Ayanz turbine stops rotating as a result of almost no wind affecting the blades. This fact makes a big difference because in 42-(b), the turbine needs to start rotating again, having to surpass the initial inertia to start rotating and having again an initial transitory which makes a big energy lost.

The case for Figure 42-(c) and 42-(d) is quite similar to the previously mentioned. However, it presents some little differences. In this case, the gust lasts 100 seconds which makes it much larger. Thus, same phenomena that happens in previous case appear in this one. The orientation time is a bit longer, approximately of 7 seconds, because the wind speed reference does not grow as fast as in the other case. For the 42-(c), the Ayanz turbine does not stop rotating as in the previous case and the only energy lost, occurs in the first 7 seconds needed for correct alignment with the wind's direction. Nevertheless, the energy lost is minimal. Conversely, the 42-(d) stops rotating during the orientating process and when it reaches the alignment with the wind, it needs to start-up again, making it lose big amount of energy.

In Table 5, the previously mentioned results are summarized. For the cases of 45° of disorientation compared to their respective wind gust 15° disorientated cases, the power peak is smaller and the total obtained energy is also smaller.

Table 5. Amount of energy generated by each orientation at each wind profile.

| Energy and peak of power generated during the test | |
|--|-------------|
| Wind speed profile | Pseudo-MPPT |
| 10sec + 10sec wind gust, 15 ° disoriented | E= 6.08 J |

Commented [MDP11]: Table 5 caption number is duplicate. Please revise.

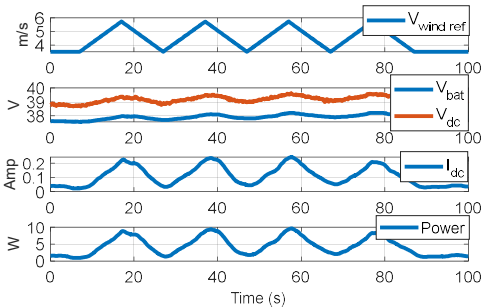
| | |
|---|---|
| | $P_{peak} = 6.67\text{ W}$ |
| 10sec + 10sec wind gust, 45 ° disoriented | $E = 2.73\text{ J}$ $P_{peak} = 4.4\text{ W}$ |
| 50sec + 50sec wind gust, 15 ° disoriented | $E = 34.36\text{ J}$ $P_{peak} = 9.63\text{ W}$ |
| 50sec + 50sec wind gust, 45 ° disoriented | $E = 31.84\text{ J}$ $P_{peak} = 10.22\text{ W}$ |

Although there are losses for both cases (20 second gust and 100 second gust), these are much notorious for the 20 second gust. So, if the gusts are fast and change their direction a significant number of degrees, the generated energy and peak power is decreased.

5.5. Performance at at Repetitive Wind Gusts

The following test consist on repetitive wind gusts with no change in its direction. This laboratory test is a simplification of the repetitive wind gusts that can be found in many city areas. Due to practical reasons, the real winds present at the cities are not possible to be reproduced with the available wind maker, so this repetitive wind profile has been used as a simplified aproximation of the real winds of the cities. For these tests, the power conversion system that is going to be used is the Pseudo-MPPT.

Figure 43 shows the behaviour of the Ayanz turbine at repetitive wind gusts. These gusts have been of 20 seconds, 10 seconds and 5 seconds, and for each test 4 of these have been reproduced. The case for Figure 43-(a) is the one where the system reaches the peak power without any troubles and follows the wind reference perfectly. It can be seen that the power peak almost reaches de 10W for all the gusts. For the case of the Figure 43-(b), the system starts to have issues to reach the maximum power that can be achieved (Figure 43-(a)), reaching to 7.5W in three gusts and to 9W in one of them. It can also be seen that the shapes of the power curves that appear tend to become smoother. For the last case, in figure 43-(c) the worst power performance generation curves are obtained. The dynamics of the current and power so fast, that the power peak is reduced substantially reaching a maximum of 6.5W for the best case, which makes a big difference with the 10W it can really extract.



(a)

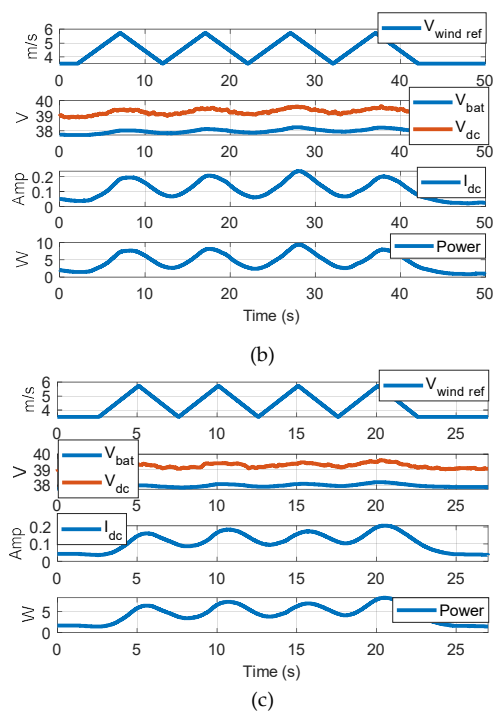


Figure 43. Performance of the Ayanz Wind Turbine with screw blades at repetitive wind gusts tests, with Pseudo-MPPT power conversion system with $L=38\text{mH}$. (a) 10sec + 10sec repetitive wind gust, (b) 5sec + 5sec repetitive wind gust, (c) 2.5sec + 2.5sec repetitive wind gust.

6. Final Discussion

6.1 Variable Wind Speed Conditions and Turbine Performances

Finally, in this section a short discussion is provided taking into consideration the results obtained and shown along the paper. First of all, it has been shown that typical wind curves provided by manufacturers at steady-state winds [35], are not enough to evaluate the generated energy at city performances. As graphically illustrated in Figure 44, the steady-state power vs wind speed curves often provided to know the energy production, are not sufficient to accurately estimated this energy of small-wind turbines located at places where gusty winds are more common. Considering the small inertias of such type of small turbines, they can often follow quite accurately many dynamics of the wind profile, providing a proportional extra energy generation than higher power wind turbines (with higher inertias due to their bigger dimensions).

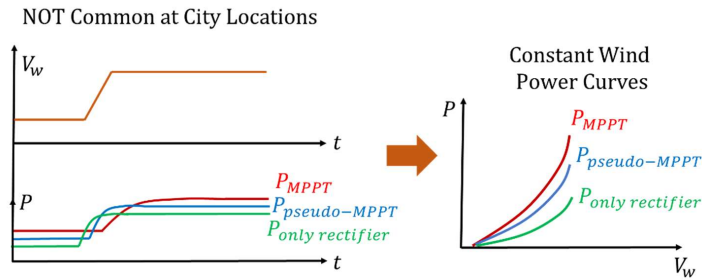


Figure 44. Wind profiles in which constant wind speed is maintained at steady-state and consequent wind-power curves provided by wind turbine manufacturers. Note that these type of wind profiles are not typical at city locations.

Regarding to the most appropriate power conversion system for a small-wind turbines, it is difficult to conclude definitively. As observed in simulation and experimental based analyses performed in previous sections and graphically simplified in Figure 45, there can be many situations and contexts, in which a given specific MPPT could be better, or a Pseudo-MPPT could be better, or even an Only-Rectifier power conversion topology could be better as well.

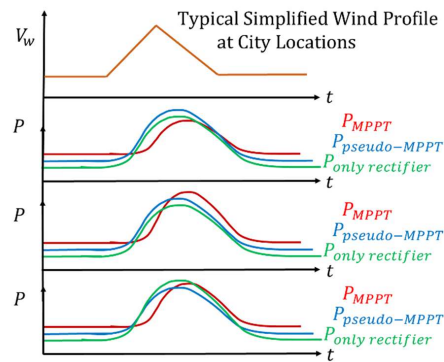


Figure 45. Some examples (not all possible ones) of the power-energy generation situations that can occur with typical simplified ‘ramp-based’ wind profiles.

Depending on many factors, it is not discardable that any of the three studied topologies could be the best extracting energy from the wind. The most determinant factors could be the ones covered at Table 5.

Table 5. Most determinant factors for maximizing the energy extracted from the wind in small-wind turbines.

| Main characteristic to maximize the energy generation |
|---|
| type of wind gusts incident at the wind turbine: slow up-down winds are preferable to be followed by the wind turbine |
| low inertia of the turbine |
| non-peaked $C_p(\lambda)$ curve (wide λ range of high C_p values) |
| starting-up torque (at zero speed) characteristic of the wind turbine (not studied at this article) |
| quick orientation of the turbine to the wind changing direction |
| small parasitic impedances of the electric generator that improves dynamic response |
| DC bus voltage utilized at the fixed voltage DC side (voltage of battery) according to the wind turbine aerodynamic characteristic in Only-Rectifier and Pseudo-MPPT configurations |
| reduction of electric losses of generator and power conversion system (including microprocessor and sensor's losses at MPPT configuration) |
| Etc. |

Finally, Figure 46 shows an example of additional information that could be provided by Small Wind Turbines to be placed at city locations affected by varying wind speeds. This information could complement the typical power vs wind speed curves provided by manufacturers, in order to more accurately know their energy production in a specific location. Thus, with these types of curves, it will be possible to know how much energy extracts a specific wind turbine, under wind gusts of different durations, knowing easily if the turbine has been designed for reasonably follow such kind of wind gusts.

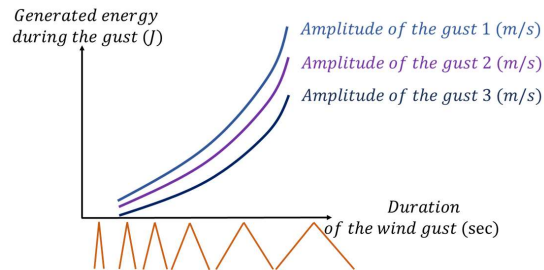


Figure 46. Additional information that could be provided by Small Wind Turbines (normally present much smaller inertia than high power three bladed wind turbines) to be placed at city locations with varying wind speeds.

6.2. Inertia Comparison of Different wind Turbines

In this sub-section, an approximative inertia evaluation of the most relevant small wind turbine morphologies is carried out. There is an uncountable amount of wind turbine topologies at the market, but for this inertia evaluation analysis only the most typical and relevant ones will be studied. Thus, an approximated inertia equation is provided for the four wind turbine morphologies studied, in function of the geometrical dimensions of the turbine as well as the density of the material used for the blade's materialization. For simplicity, several assumptions and simplifications are done, so the obtained mathematical expressions for the inertia values are sufficiently simple and manageable. Basically, the main assumption is that the blade shape or geometry is simplified to a 'similar' shape in which the inertia expression is well known already. Then also, only blades are considered at the inertia calculation, while other elements necessary for their assembly are neglected: shafts, hubs, screws and tie rods, etc. The small-wind turbines considered present three blades, for equal comparative purposes. But a different number of blades can be also evaluated with the expressions derived.

Hence, the first small wind turbine considered is obviously, the one utilized at this paper, i.e. the Ayanz wind turbine with screw blades. As has been shown, the screw blades utilized at the analysis of the paper, are the Spiral Archimedes shape [22,23,29]. Figure 47 illustrates a simplified representation of one of the blades and the equivalent inertia expression derived. Note again that the shaft is ideally considered with zero radio, which implies that the blade starts at zero angle ϑ .

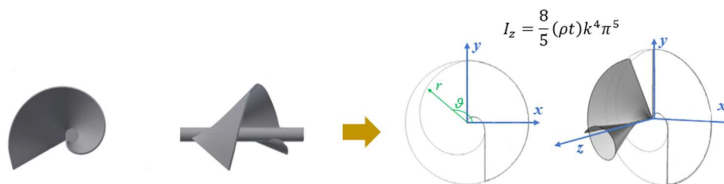


Figure 47. Simplified representation of a Spiral Archimedes blade in a 3-Bladed Horizontal axis Ayanz Wind Turbine with screw blades.

In polar coordinates, the radio of the spiral blade projection at the x-y plane can be expressed as [29]:

$$r = k \cdot \theta \quad (6)$$

Being k , a real number. Changing the parameter k the distance between loops is modified. Here, it is assumed that the mass particles of the blade projected to the x-y plane, resulting the Archimedean Spiral, present the same distance to the z axis as the original three-dimensional blade mass particles. Then, the differential mass is derived as [36]:

$$dm = (\rho t) dA = (\rho t)(r dr d\theta) \quad (7)$$

With ρ the density of the material employed and t , the thickness of the blade.

$$I_z = \int_0^{k\theta} r^2 dm = \int_0^{k\theta} \int_0^{2\pi} r^2 (\rho t)(r dr d\theta) \quad (8)$$

Which results in:

$$I_z = \frac{8}{5} (\rho t) k^4 \pi^5 \quad (9)$$

Thus, for this type of blade geometry, the highest radio of the spiral determined by k , the maximum angle 2π ($r = k \cdot 2\pi$) and the density ρ determines the inertia of one of the blades. Then, in order to calculate the total inertia of the 3 blades, this value must be simply multiplied by 3.

Then, the second type of wind turbine considered is the classic horizontal axis 3-Bladed wind turbine. At this time, the geometry of the complex geometry of an airfoiled profile is simplified to a rectangular prism of thickness t as depicted in Figure 48. It can be considered as a family of wind turbines, depending on the number of blades employed.

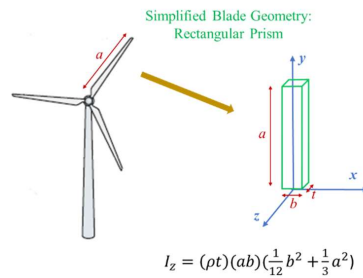


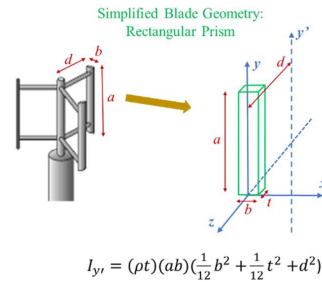
Figure 48. Simplified representation of a horizontal axis 3-Bladed wind turbine.

In this case, the equivalent inertia across the z axis of a rectangular prism geometry is of common knowledge and is equal to [36]:

$$I_z = (\rho t)(ab)(\frac{1}{12}b^2 + \frac{1}{3}a^2) \quad (10)$$

Again, in order to calculate the total inertia of the 3 blades, this value should be simply multiplied by 3.

Then, in Figure 49, the 3rd type of small wind turbine morphology is illustrated. It is a vertical axis 3-Bladed Darrieus type wind turbine, firstly patented a century ago by Darrieus [37]. For simplicity and because many commercial turbines of this type do in this way, the curvature or oval shape of the blades has not been considered. Hence, as can be noticed at Figure 49, again the complex geometry of an airfoiled profile is simplified to a rectangular prism of thickness t .



$$I_{y'} = (\rho t)(ab)\left(\frac{1}{12}b^2 + \frac{1}{12}t^2 + d^2\right)$$

Figure 49. Simplified representation of a vertical axis 3-Bladed Darrieus type wind turbine.

In this case, again as before, the equivalent inertia across the y axis of a so simple geometry is of common knowledge and is equal to [36]:

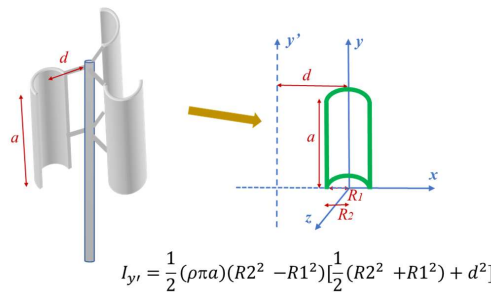
$$I_y = \frac{1}{12}(\rho t)(ab)(b^2 + t^2) \quad (11)$$

While the inertia across the parallel axis y' , by using the Steiner theorem is [36]:

$$I_{y'} = (\rho t)(ab)\left(\frac{1}{12}b^2 + \frac{1}{12}t^2 + d^2\right) \quad (12)$$

Note that the distance d to the shaft, strongly affects to the inertia compared to the other two parameters b and t , which are divided by a factor of 12. This is due to the fact that all the mass of the blade is concentrated to a distance d to the shaft. So, if this distance is 'high', the tendency of the equivalent inertia will be 'high' as well.

Finally, the last family of small wind turbines is named as Vertical Axis Ayanz-Savonius wind turbines, being consequent with their corresponding respective patents of XVII century (Ayanz-[18]) and XX century (Savonius-[38]). In Figure 50, a simplified representation of a vertical axis 3 bladed wind turbine of this type is depicted. The blades are placed to a distance d to the shaft (more like in the Ayanz patent, rather than in Savonius patent). In this case, the geometry of the blades are half cylinders of internal and external radii $R1$ and $R2$.



$$I_{y'} = \frac{1}{2}(\rho \pi a)(R2^2 - R1^2)\left[\frac{1}{2}(R2^2 + R1^2) + d^2\right]$$

Figure 50. Simplified representation of a Vertical Axis Ayanz-Savonius 3-Bladed wind turbine (*Note that the Savonius patent and Ayanz patent present differences, but the most relevant one is that the Savonius patent considers an embrace of the blades to the central shaft, while in Ayanz patent, the blades are fixed with rods to a distance of the shaft).

Thus, again as in previous case, the equivalent inertia across the y axis of a so simple geometry is of common knowledge and is equal to [36]:

$$I_y = \frac{1}{4}(\rho \pi a)(R2^4 - R1^4) \quad (13)$$

While again, the inertia across the parallel axis y' , by using the Steiner theorem is [36]:

$$I_{y'} = \frac{1}{2}(\rho \pi a)(R2^2 - R1^2)\left[\frac{1}{2}(R2^2 + R1^2) + d^2\right] \quad (14)$$

In this particular case, the distance d compared with other parameters $R1$ and $R2$ does not increase the inertia so dramatically as in previous Darrieus type turbines, since the mass of the blades is distributed across the distance $d-R2$ to $d+R2$.

Finally, a quantitative comparison is carried out for the four types of small wind turbines previously modelled. It is almost impossible to perform a fair comparison, between four so different morphologies of turbines, so the results have to be taken with caution or at least comprehensively. Thus, the comparative framework adopted considers equal area of wind incidence for each wind turbine. What means that for the horizontal axis wind turbines circular area of incidence of the air is considered, while for the vertical axis wind turbines rectangular area is considered. Table 6 shows the areas, proportions and values that have been considered.

Table 6. Wind incident areas, proportions and parameter’s values that have been considered for each wind turbine. Material of the blades: aluminium, density =2700kg/m³.

| | Incident Wind Area | t (m) | - | - |
|---|-----------------------|-------|------|-----------|
| Ayanz Wind Turbine with screw blades | $\pi(k \cdot 2\pi)^2$ | 0.003 | - | - |
| $I_z = \frac{8}{5}(\rho t)k^4\pi^5$ | | | | |
| | Incident Wind Area | t (m) | b | - |
| Horizontal Axis 3-Bladed | $\pi(a)^2$ | 0.009 | 0.2a | - |
| $I_z = (\rho t)(ab)(\frac{1}{12}b^2 + \frac{1}{3}a^2)$ | | | | |
| | Incident Wind Area | t (m) | b | d |
| Vertical Axis 3-Bladed Darrieus | 2da | 0.006 | 0.2a | (1/3)a |
| $I_{y'} = (\rho t)(ab)(\frac{1}{12}b^2 + \frac{1}{12}t^2 + d^2)$ | | | | |
| | Incident Wind Area | t (m) | d | a |
| Vertical Axis 3-Bladed Ayanz-Savonius | 2a(d + R2) | 0.003 | 2R2 | 2(d + R2) |
| $I_{y'} = \frac{1}{2}(\rho \pi a)(R2^2 - R1^2)[\frac{1}{2}(R2^2 + R1^2) + d^2]$ | | | | |

It is noticed that each wind turbine presents different thickness and proportions of geometries. It has been treated to be closer to a realistic practical design as possible. Nevertheless, if the reader wants to use different parameters and proportions, all the mathematical formulations can be adapted. Finally, it has to be remarked that for the Ayanz-Savonius vertical axis wind turbine, the proportions considered are as proposed at the original Ayanz patent [18]. Hence, four different incident wind areas are considered, applied to the 4 wind turbines with proportions and parameter’s values of Table 6. The resulting inertias are provided in Figure 51.

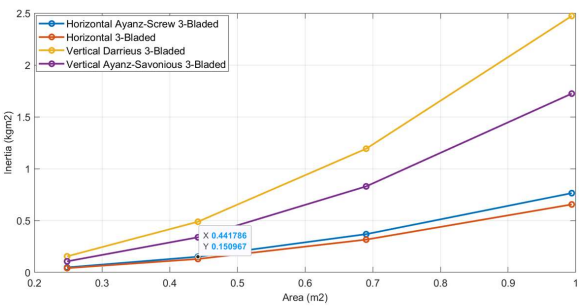






Figure 51. Inertias evaluated according to the simplified expressions provided, considering equal wind incident areas in four wind turbines. Areas (m²): [0.24,0.44,0.69,0.99].

It can be noticed that the vertical axis wind turbines present higher inertias than the horizontal axis ones and this difference becomes greater with higher areas. This is due to the fact that the majority mass of their blades is concentrated around a distance d to the shaft. If different proportions and geometries' values are used, the resulting inertias would change. However, this is a reasonably good first approach to better understand the intrinsic natural inertia values of different wind turbines.

6.3. General Qualitative Performance of Different Small Wind Turbines

To conclude this section provides a comparison of general qualitative performance of different wind turbines. Table 7 shows the performance of several objectives that should seek different wind turbine designs. The most commonly used small wind turbines have been classified in 4 four main groups as in previous sub-section. It can be noticed that the Ayanz Wind Turbine with screw blades employed in this article, is very well positioned among typical small wind turbines. Thus, in terms of maximum achievable C_{pmax} , probably the horizontal axis with airfoiled blades is the best, then would come the Darrieus type turbines, then the Ayanz with screw blades and finally the drag type vertical axis ones. However, as has been shown in this article, this C_{pmax} alone is not the most determinant factor to maximize the generated energy. This factor, should be accompanied by a low inertia of the wind turbine. As has been shown, in principle, the inertia of vertical axis wind turbines is higher than the horizontal axis ones. Then, regarding the electric losses of the turbine, depends only on the electronic conversion system used and does not depend on the turbine's geometry. While the peaked shape of the $C_p(\lambda)$ curve is an issue that could not be studied in this article due to lack of information. Regarding to the start-up torque characteristic, probably the drag type vertical axis ones and Ayanz with screw blades could be the best. In relation to the maximization of the generated energy at winds that change often the direction, the vertical axis wind turbines are well positioned. Probably the horizontal axis with airfoiled blades presents the worst performance since the vane is normally located behind the blades and therefore, they are moved by de-energized winds in comparison with the Ayanz with screw blades. Then, the Ayanz with screw blades is clearly the best positioned in minimization the visual impact and acoustic noise, minimization of birds casualties and on safety in case of blade failure. On the contrary, the worst positions in these four indicators are horizontal axis turbines with airfoiled blades. Finally, in relation to the last two indicators of Table 7, the authors can not conclude convincingly, since it is something out of scope of this article, but it should be considered for future works.

Table 7. General Qualitative Performance of Different Small Wind Turbines.

| Objective | Drag type vertical axis Ayanz- Savonius | Ayanz with screw blades | Vertical Axis Darrieus | Horizontal axis |
|--|---|---|---|--|
| |  |  |  |  |
| Maximize the generated energy at variable (gusty) winds: | | | | |
| -High C_{pmax} natural characteristic | - | + | + | ++ |
| -Low inertia | - | + | - | + |
| - Non-peaked $C_p(\lambda)$ curve | ? | ? | ? | ? |

| | | | | |
|--|----|----|----|----|
| - Reduction of electric losses | + | + | + | + |
| Maximize the generated energy at low-speed winds (good start-up torque characteristic) | + | + | - | - |
| Maximize the generated energy at winds that change often the direction (quick orientation in horizontal axis turbines) | ++ | + | ++ | - |
| Minimize the visual impact (mainly avoid seeing the blades rotating) | + | ++ | - | -- |
| Minimize the acoustic noise impact (minimize noise due to fast rotations of blades) | + | + | - | -- |
| Maximize prevention of birds’ deaths | + | ++ | - | - |
| Maximize safety in case of destructive failure of blades | - | ++ | -- | -- |
| Maximize reliability of the Wind Turbine (low mechanical stress due to low rotational speed and Blades are protected from rain) | + | ++ | + | + |
| Maximize the possibility to do easy and cheap designs | ? | ? | ? | ? |
| Maximize environmentally friendly construction designs and smart recyclability | ? | ? | ? | ? |

Author Contributions: Conceptualization, G.A. and A.P.; methodology, G.A.; software, G.A., A. P and G.K; validation, A.P., G. A and G.K; formal analysis, A.P., G. A and G.K; investigation, G.A. and A.P.; resources, G.A.; data curation, A.P.; writing—original draft preparation, G.A. and A.P.; writing—review and editing, G.A. and A.P.; visualization, G.A. and A.P.; supervision, G.A.; project administration, G.A.; funding acquisition, G.A. All authors have read and agreed to the published version of the manuscript.”.

References

1. Buri, Z.; Sipos, C.; Szűcs, E.; Máté, D. Smart and Sustainable Energy Consumption: A Bibliometric Review and Visualization. *Energies* **2024**, *17*, 3336. <https://doi.org/10.3390/en17133336>.

2. Wardal, W.J.; Mazur, K.; Barwicki, J.; Tseyko, M. Fundamental Barriers to Green Energy Production in Selected EU Countries. *Energies* **2024**, *17*, 3664. <https://doi.org/10.3390/en17153664>.

3. Zidane, T.E.; Aziz, A.L.; Zahraoui, Y.; Kotb, H.; AboRas, K.M.; Kitmo; Jember, Y.B. Grid-Connected Solar PV Power Plants Optimization: A Review. *IEEE*. 2023, Volume 11, pp. 79588-79608.

4. Pater, S. Increasing Energy Self-Consumption in Residential Photovoltaic Systems with Heat Pumps in Poland. *Energies* **2023**, *16*, 4003. <https://doi.org/10.3390/en16104003>.

5. Liu, H.-Y.; Skandalos, N.; Braslina, L.; Kapsalis, V.; Karamanis, D. Integrating Solar Energy and Nature-Based Solutions for Climate-Neutral Urban Environments. *Solar* **2023**, *3*, 382-415. <https://doi.org/10.3390/solar3030022>.

6. Boudjemai, H.; Ardjoun, S.A.E.M.; Chafouk, H.; Denai, M.; Elbarbary, Z.M.S.; Omar, A.I.; Mahmoud, M.M. Application of a Novel Synergetic Control for Optimal Power Extraction of a Small-Scale Wind Generation System with Variable Loads and Wind Speeds. *Symmetry* **2023**, *15*, 369. <https://doi.org/10.3390/sym15020369>.

7. Stepaniuk, V.; Pillai, J.R.; Bak-Jensen, B.; Padmanaban, S. Estimation of Energy Activity and Flexibility Range in Smart Active Residential Building. *Smart Cities* **2019**, *2*, 471-495. <https://doi.org/10.3390/smartcities2040029>.

8. Ramadan, R.; Huang, Q.; Zalhaf, A.S.; Bamişile, O.; Li, J.; Mansour, D.-E.A.; Lin, X.; Yehia, D.M. Energy Management in Residential Microgrid Based on Non-Intrusive Load Monitoring and Internet of Things. *Smart Cities* **2024**, *7*, 1907-1935. <https://doi.org/10.3390/smartcities7040075>.

9. Mortensen, L.K.; Shaker, H.R. Data-Driven Reliability Prediction for District Heating Networks. *Smart Cities* **2024**, *7*, 1706-1722. <https://doi.org/10.3390/smartcities7040067>.

10. Hammoumi, L.; Maanan, M.; Rhinane, H. Characterizing Smart Cities Based on Artificial Intelligence. *Smart Cities* **2024**, *7*, 1330-1345. <https://doi.org/10.3390/smartcities7030056>.

11. Lazaroiu, A.C.; Gmal Osman, M.; Strejoiu, C.-V.; Lazaroiu, G. A Comprehensive Overview of Photovoltaic Technologies and Their Efficiency for Climate Neutrality. *Sustainability* **2023**, *15*, 16297. <https://doi.org/10.3390/su152316297>.
12. Pu, O.; Yuan, B.; Li, Z.; Bao, T.; Chen, Z.; Yang, L.; Qin, H.; Li, Z. Research on the Characteristics of Urban Building Cluster Wind Field Based on UAV Wind Measurement. *Buildings* **2023**, *13*, 3109. <https://doi.org/10.3390/buildings13123109>.
13. Corbalán, P.A.; Chiang, L.E. Fast Power Coefficient vs. Tip-Speed Ratio Curves for Small Wind Turbines with Single-Variable Measurements following a Single Test Run. *Energies* **2024**, *17*, 1199. <https://doi.org/10.3390/en17051199>.
14. Ramos-Paja, C.A.; Henao-Bravo, E.E.; Saavedra-Montes, A.J. MPPT Solution for Commercial Small Wind Generation Systems with Grid Connection. *Energies* **2023**, *16*, 719. <https://doi.org/10.3390/en16020719>.
15. Zagubień, A.; Wolniewicz, K. Energy Efficiency of Small Wind Turbines in an Urbanized Area—Case Studies. *Energies* **2022**, *15*, 5287. <https://doi.org/10.3390/en15145287>.
16. Rosato, A.; Perrotta, A.; Maffei, L. Commercial Small-Scale Horizontal and Vertical Wind Turbines: A Comprehensive Review of Geometry, Materials, Costs and Performance. *Energies* **2024**, *17*, 3125. <https://doi.org/10.3390/en17133125>.
17. Castillo, O.C.; Andrade, V.R.; Rivas, J.J.R.; González, R.O. Comparison of Power Coefficients in Wind Turbines Considering the Tip Speed Ratio and Blade Pitch Angle. *Energies* **2023**, *16*, 2774. <https://doi.org/10.3390/en16062774>.
18. Abad, G.; Zarketa-Astigarraga, M.P.Y.A. Molinos de Viento Patentados por Jerónimo de Ayanz y Beaumont en el año 1606; un Análisis Conceptual Desde una Perspectiva Ingenieril del Año 2021; Mondragon Unibertsitatea: Mondragon, Spain, 2021.
19. Tapia, N.G. Jerónimo de Ayanz y Beaumont. Un Inventor Navarro (1553-1613); Universidad Pública de Navarra: Pamplona, Spain, 2010.
20. Liam F1 Archimedes AWM-750D-150W Datasheet. (Liam F1 Archimedes). Available online at <https://thearchimedes.com/>
21. Song, K.; Huan, H.; Kang, Y. Aerodynamic Performance and Wake Characteristics Analysis of Archimedes Spiral Wind Turbine Rotors with Different Blade Angle. *Energies* **2023**, *16*, 385. <https://doi.org/10.3390/en16010385>.
22. Abdelaziz G. Refaie, H.S. Abdel Hameed, Mohamed A.A. Nawar, Youssef A. Attai, Mohamed H. Mohamed, Comparative investigation of the aerodynamic performance for several Shrouded Archimedes Spiral Wind Turbines, Energy, Volume 239, Part C, 2022, 122295, ISSN 0360-5442, <https://doi.org/10.1016/j.energy.2021.122295>.
23. Kim, K.; Ji, K.; Kim, H.Y.; Lu, Q.; Baek, J. Experimental and Numerical Study of the Aerodynamic Characteristics of an Archimedes Spiral Wind Turbine Blade. *Energies* **2014**, *7*, 7893–7914.
24. Refaie, A.G.; Hameed, H.A.; Nawar, M.A.; Attai, Y.A.; Mohamed, M.H. Qualitative and quantitative assessments of an Archimedes Spiral Wind Turbine performance augmented by a concentrator. *Energy* **2021**, *231*, 121128.
25. Jang, H.; Kim, D.; Hwang, Y.; Paek, I.; Kim, S.; Baek, J. Analysis of Archimedes Spiral Wind Turbine Performance by Simulation and Field Test. *Energies* **2019**, *12*, 4624.
26. Arzuaga, A.; Estivariz, A.; Fernández, O.; Gubía, K.; Plaza, A.; Abad, G.; Cabezuero Romero, D. Low-Cost Maximum Power Point Tracking Strategy and Protection Circuit Applied to an Ayanz Wind Turbine with Screw Blades. *Energies* **2023**, *16*, 6204. <https://doi.org/10.3390/en16176204>.
27. Micallef, D.; Van Bussel, G. A Review of Urban Wind Energy Research: Aerodynamics and Other Challenges. *Energies* **2018**, *11*, 2204. <https://doi.org/10.3390/en11092204>.
28. Marrone, P.; Fiume, F.; Laudani, A.; Montella, I.; Palermo, M.; Fulginei, F.R. Distributed Energy Systems: Constraints and Opportunities in Urban Environments. *Energies* **2023**, *16*, 2718. <https://doi.org/10.3390/en16062718>.
29. Article from Wikipedia: https://en.wikipedia.org/wiki/Archimedean_spiral
30. J. G. Njiri y D. Söffker, “State-of-the-art in wind turbine control: Trends and challenges,” in *Renewable and Sustainable Energy Reviews*, Vol. 60, 2016.
31. G. Abad et al, Doubly Fed Induction Machine: Modelling and Control for Wind Energy Generation, Wiley-IEEE Press, ISBN: 9780470768655, 2011.
32. Bin. Wu et al, Power Conversion and Control of Wind Energy Systems, Wiley-IEEE Press, ISBN: 978-1-118-02899-5, 2011.
33. J. L. R. Amenado, Sistemas eólicos de producción de energía eléctrica, Rueda SL, ISBN; 8472071391, 2003.
34. Camblong, H. Experimental evaluation of wind turbines maximum power point tracking controllers. *Energy Conversion and Management*. 2006. 47. DOI: 10.1016/J.ENCONMAN.2006.03.033.
35. Standard: IEC 61400-1:2019.
36. F. P. Beer, Vector mechanics for engineers. Statics and dynamics, *Mc Graw Hill*, 978-0-07-339824-2, 1995.

37. US Patent (US1835018): G. J. M. Darrieus, Turbine Having its rotating shaft transverse to the flow of the current. 1925.
38. US Patent (US311793): S. J. Savonius, Wind Rotor, 1930.

Disclaimer/Publisher's Note: The statements, opinions and data contained in all publications are solely those of the individual author(s) and contributor(s) and not of MDPI and/or the editor(s). MDPI and/or the editor(s) disclaim responsibility for any injury to people or property resulting from any ideas, methods, instructions or products referred to in the content.